Probing the Requirements for Dual Angiotensin-Converting Enzyme C-Domain–Selective/Neprilysin Inhibition

Lauren B. Arendse[†,‡,+], Gyles E. Cozier[±,+], Charles J. Eyermann[⊥], Gregory S. Basarab[⊥], Sylva L. Schwager[†,‡], Kelly Chibale[†,⊥,§,‖], K. Ravi Acharya[±,*], Edward D. Sturrock[†,‡,*]

[†]Institute of Infectious Disease and Molecular Medicine, University of Cape Town, Observatory 7925, South Africa

[‡]Department of Integrative Biomedical Sciences, University of Cape Town, Observatory 7925, South Africa

[±]Department of Biology and Biochemistry, University of Bath, Claverton Down, Bath BA2 7AY, United Kingdom

[⊥]Drug Discovery and Development Centre (H3D), University of Cape Town, Rondebosch 7701, South Africa

[§]Department of Chemistry, University of Cape Town, Rondebosch 7701, South Africa

[‖]South African Medical Research Council Drug Discovery and Development Research Unit, University of Cape Town, Rondebosch 7701, South Africa

[+]Authors with equal contribution

[*]Joint corresponding authors. E-mail: Edward D. Sturrock edward.sturrock@uct.ac.za; K. Ravi Acharya bsskra@bath.ac.uk

ABSTRACT

Selective inhibition of the angiotensin-converting enzyme C-domain (cACE) and neprilysin (NEP), leaving the ACE N-domain (nACE) free to degrade bradykinin and other peptides, has the potential to provide the potent antihypertensive and cardioprotective benefits observed for non-selective dual ACE/NEP inhibitors, such as omapatrilat, without the increased risk of adverse effects. We have synthesized three 1-carboxy-3-phenylpropyl dipeptide inhibitors with nanomolar potency based on the previously reported C-domain selective ACE inhibitor lisinopril-tryptophan (LisW) to probe the structural requirements for potent dual cACE/NEP inhibition. Here we report the synthesis, enzyme kinetic data and high-resolution crystal structures of these inhibitors bound to nACE and cACE, providing valuable insight into the factors driving potency and selectivity. Overall, these results highlight the importance of the interplay between the S_1' and S_2' subsites for ACE domain selectivity, providing guidance for future chemistry efforts towards the development of dual cACE/NEP inhibitors.

INTRODUCTION

The therapeutic blockade of the renin–angiotensin system (RAS) using angiotensin-converting enzyme (ACE) inhibitors and angiotensin receptor blockers (ARBs) has been a mainstay for the treatment of hypertension, the main risk factor for cardiovascular disease. Despite the success of ACE inhibitors and ARBs, RAS blockage in many cases, does not lead to adequate reduction in blood pressure and there is still a need for new approaches for the treatment of hypertension and cardiovascular disease.[1] There is ongoing interest in developing therapeutics that modulate multiple interconnected vasoactive pathways controlling blood pressure and cardiovascular function to improve blood pressure management.[2]

Towards developing such improved therapeutics, dual ACE and neprilysin (NEP) inhibitors, which exploit the structural similarity between these zinc peptidases, were developed to block the ACE-mediated conversion of Angiotensin (Ang) I to the vasoconstrictor Ang II and the NEP-mediated degradation of natriuretic peptide vasodilators. The combination of key features from the early specific ACE and NEP inhibitors, namely the P_2' proline group a common feature in ACE inhibitors and a P_1' benzyl group that is important for NEP inhibition, led to mercaptoacyl dipeptides with potent dual ACE/NEP inhibitory activity.[3-5] Fused heterocyclic dipeptide mimetics were introduced in further optimisation steps to improve in vivo activity, leading to the 7,6-fused bicyclic thiazepinone, omapatrilat (**Figure 1A**).[6] Omapatrilat showed great promise in experimental models of hypertension and heart failure, and early clinical studies demonstrated better antihypertensive activity and cardioprotective effects than other drug classes.[7-14] Despite this initial promise, omapatrilat failed to obtain U.S. Food and Drug Administration (FDA) approval due to an increased rate of angioedema when compared to the standard ACE inhibitor enalapril during Phase III clinical trials.[15-18] ACE and NEP both contribute to the breakdown of multiple vasoactive peptides, including bradykinin. Accumulation of bradykinin and other vasopeptidase substrates (e.g. endothelin-1) has been linked to angioedema and other adverse side effects.[19, 20] Dual inhibition of both ACE and NEP, although highly effective at reducing blood pressure, is thought to lead to compounding adverse effects due to the involvement of these enzymes in bradykinin metabolism.[20, 21] Due to this risk, and the unfortunate end to the development of omapatrilat, large-scale trials of other clinical candidates in this drug class have not been carried out.

Early ACE and NEP inhibitors were designed without the benefit of high-resolution protein structures of the targets or insights into the unique roles of the individual ACE domains. There are two isoforms of ACE, somatic ACE and testes ACE. Somatic ACE consists of two homologous catalytic domains, the N-domain (nACE) and the C-domain (cACE), while testes ACE consists of a single catalytic domain, corresponding to cACE of somatic ACE. Despite high homology, nACE and cACE display distinct substrate specificity and have different but overlapping functions. It is now well established that cACE is primarily responsible for the conversion of Ang I to Ang II and is adequate and essential for controlling blood pressure in vivo.[22-25] nACE is the primary site for cleavage of other peptides including the potent antifibrotic and anti-inflammatory peptide N-acetyl-Ser–Asp–Lys–Pro (Ac-SDKP).[24, 26] In contrast, both nACE and cACE metabolise bradykinin at similar rates, and either domain is sufficient to compensate for the absence of the other.[22, 25] This knowledge has led to the development of both nACE and cACE selective inhibitors.[27-33] In vitro inhibition data combined with site-directed mutagenesis, high-resolution structures of individual nACE and cACE proteins, and molecular dynamic simulations have provided insights into the role of domain specific active site residues, as well as more subtle differences in plasticity, which are responsible for conferring domain-selectivity.[33-39] The most advanced cACE selective inhibitor (cACEi) LisW is a derivative of the non-selective ACE inhibitor (ACEi) lisinopril (**Figure 1A**) that displays >100-fold selectivity for cACE over nACE (C-selectivity) in vitro.[32, 39] In vivo studies in rodent models of myocardial infarction and hypertension have confirmed that LisW selectively inhibits the cACE in vivo,[40] resulting in a reduction in Ang II peptide levels and blood pressure that is comparable to that achieved with lisinopril, but without increasing bradykinin levels.[41]

There is therefore considerable value in developing combination therapies or dual inhibitors that selectively target cACE and NEP, leaving nACE free to degrade bradykinin and other substrates, thus offering the benefits of dual ACE/NEP inhibition without the increased risk of adverse effects observed for omapatrilat. Indeed, omapatrilat non-selectively inhibits both the nACE and cACE, forming identical interactions within the active sites.[42, 43] Encouragingly, recent ex vivo and in vivo studies have demonstrated that a combination of LisW and the NEP inhibitor sacubitril (cACEi + NEPi) reduced vascular permeability and endothelial injury

compared to omapatrilat (dual ACEi/NEPi) and lisinopril + sacubitril (ACEi + NEPi), further supporting the development of dual cACE-selective/NEP inhibitors (cACEi/NEPi).[44]

Towards this goal, we have synthesised three novel LisW analogues to probe the structural requirements for potent dual cACE/NEP inhibition. In the present study we report the in vitro nACE, cACE and NEP inhibition data for these 1-carboxy-3-phenylpropyl N-capped dipeptides, together with high-resolution inhibitor-bound structures of nACE and cACE, providing valuable insights that contribute towards designing a single molecule capable of dual cACE/NEP inhibition.

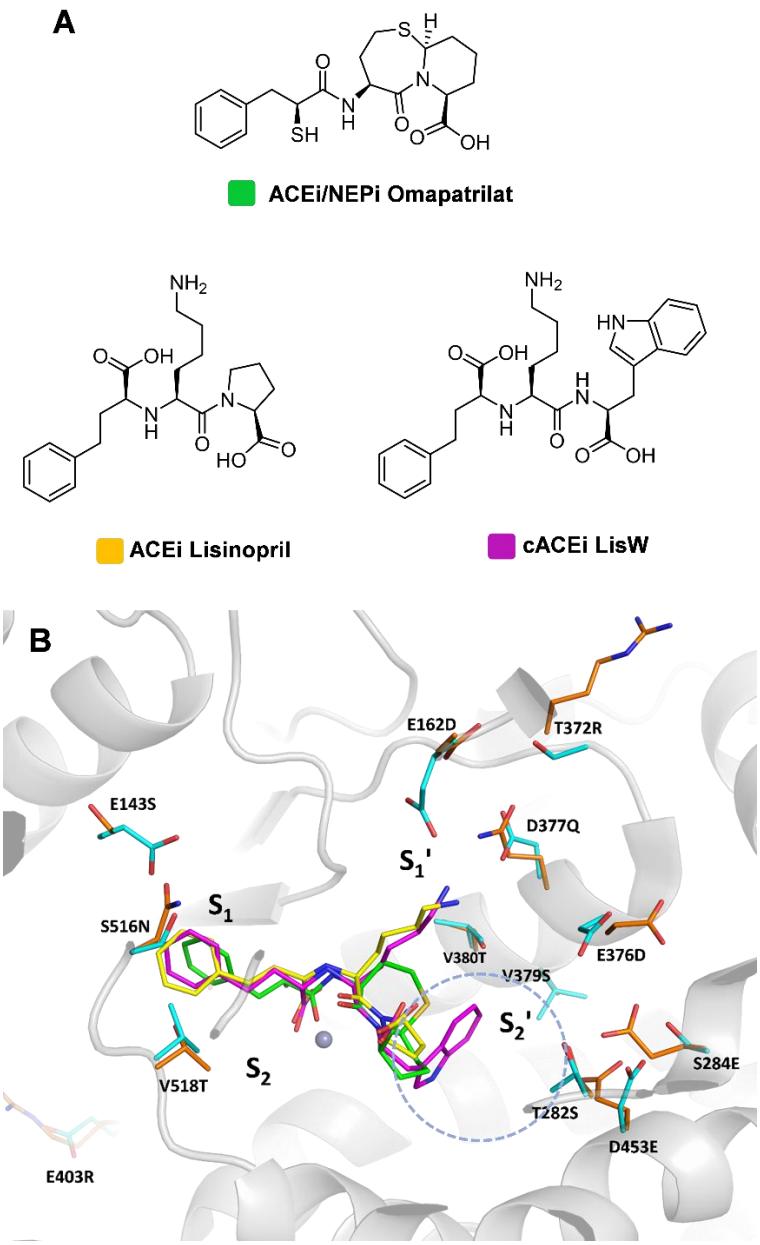

Figure 1. A) Anti-hypertensive agents omapatrilat, lisinopril and LisW (ACEi/NEPi – non-selective dual inhibitor targeting nACE, cACE and NEP; cACEi – domain selective inhibitor targeting cACE). B) Overlay of ACE crystal structures with cACE in complex with omapatrilat in green (PDB 6H5W), cACE in complex with LisW in magenta (PDB 3L3N), and nACE in complex with lisinopril in yellow (PDB 2C6N). cACE unique residues are shown in cyan (PDB 3L3N) with corresponding N-domain residues in orange (PDB 2C6N). Zinc ions are depicted as lilac spheres. PDB, Protein Data Bank.

RESULTS

Design and synthesis.

No dual cACEi/NEPi has been reported to date, but there are inhibitor-bound ACE structures for several cACE inhibitors with greater than two orders of magnitude C-selectivity (reviewed in Arendse et al[2]). The cACE inhibitors described to date have typically been derived from potent non-selective ACE inhibitors, with modifications significantly reducing nACE binding rather than enhancing cACE potency. A common feature in reported cACE inhibitors, is a bulky hydrophobic group that extends into the S_2' subsite as observed for LisW (**Figure 1B**). Inhibitor matched pairs and site-directed mutagenesis studies, in which cACE specific residues were converted to the corresponding nACE residues, have shown that the P_2' sidechain together with synergistic effects between multiple unique cACE residues in and distal to the S_2' subsite contribute significantly to the selectivity of these compounds conferring 30- to 70-fold of the observed C-selectivity.[33, 34, 39] Nevertheless, the full picture is more complex with unique interactions in other subsites as well as differences in domain plasticity also contributing to domain selectivity.[35, 38]

In NEP, the large hydrophobic prime subsites are primarily responsible for peptide binding and specificity, with the S_1' subsite preferentially binding aromatic groups or bulky hydrophobic sidechains as observed for the potent dual ACEi/NEPi acyclic mercaptoacyl dipeptides.[3, 45] In the absence of a hydrophobic sidechain at this P_1' position, as is the case for omapatrilat, an alternative binding pose is observed in NEP, where the P_1 group binds to S_1' subsite (**Figure S1**).[43, 46, 47]

Based on previous studies and the structure of LisW, three dipeptides containing an N-terminal nitrogen capped with 1-carboxy-3-phenylpropyl were synthesized to probe the requirements of the ACE and NEP prime subsites for dual cACE/NEP inhibition (**Figure 2**). The terminal

amine of the butyl sidechain was removed in LisW analogues AD011 and AD012, improving NEP inhibitory activity. In compound AD012, the P_2' tryptophan residue is replaced by a tyrosine residue.

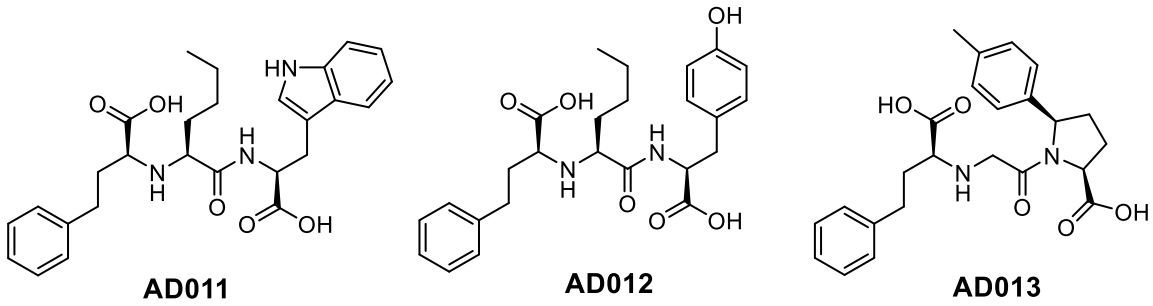

Figure 2. New LisW analogues

Compounds AD011 and AD012, were synthesized from **3** (Scheme 1) via n-propanephosphonic acid anhydride (T3P)-mediated peptide coupling with tryptophan and tyrosine methyl esters, respectively, followed by hydrolysis. Compound **3**, in turn, was derived via the reaction between bromide **1**[48] and amine **2,** followed by removal of the *t*-butyl group. Compound AD013 was derived from **8** via T3P peptide coupling of **9**[5] with **8** (Scheme 2). Compound **8** was synthesized from **6** via the reaction between amine **6** and the *t*-butyl ester of chloroacetic acid to afford **7,** followed by *t*-Boc conversion of the ester to the acid, and protection of the amine as the *t*-Boc.

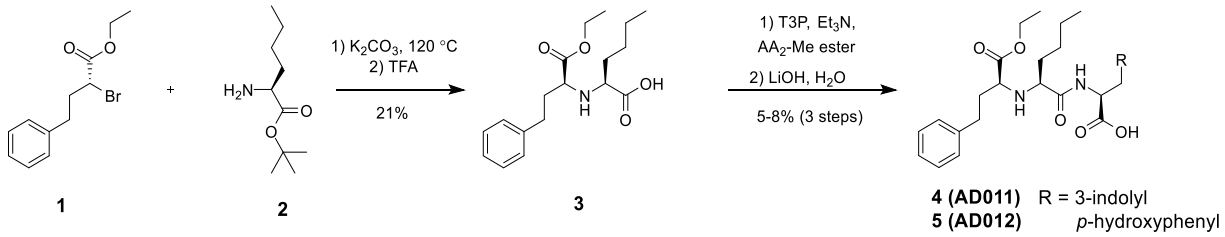

Scheme 1. Synthesis of compounds **AD011** and **AD012**

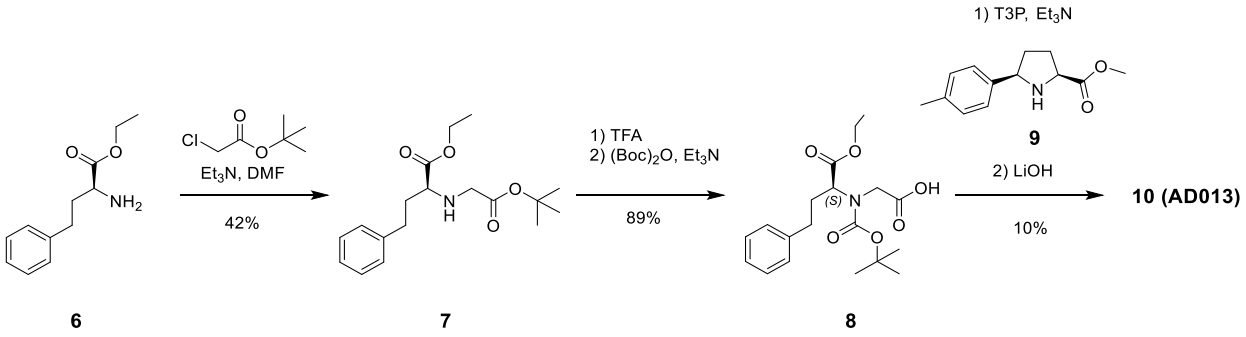

Scheme 2. Synthesis of compounds **AD013**

Enzyme Inhibition.

Compounds were tested for nACE, cACE and NEP inhibitory potency in fluorogenic-based enzyme assays using single domain recombinant human ACE proteins and the human NEP ectodomain. Enzyme inhibition kinetics conformed to the classical competitive inhibition model and K_i values were calculated from IC_{50} values using the Cheng-Prusoff equation ($K_i = IC_{50}/(1 + [S]/K_m)$) were [S] is the substrate concentration and K_m is the Michaelis-Menten constant (K_m) (**Table 1**).

Table 1. Inhibitory constants for lisinopril, LisW and related analogues

Compound	NEP K_i (µM)	nACE K_i (µM)	cACE K_i (µM)	C-selectivity factor[a]
Lisinopril [b]	n.d.	0.0048	0.0012	4
LisW	> 150	1.7	0.009	189
AD011	19	3.79	0.10	37
AD012	0.6	0.12	0.035	3.5
AD013	> 50	3.4	0.44	8

Inhibitory constants calculated using $K_i = IC_{50}/(1 + [S]/K_m)$. IC_{50} values were determined from $n \geq 2$ independent assays. [a]C-selectivity factor = nACE K_i/cACE K_i. [b]Previously reported K_i values for lisinopril.[39]

Overall nACE and cACE structures in complex with inhibitors

High-resolution crystal structures were obtained for the inhibitors AD011, AD012 and AD013 in complex with nACE (2.00, 1.60 and 1.70 Å, respectively) and cACE (1.50, 1.65 and 1.60 Å, respectively) (data processing and refinement statistics shown in **Table 2**). All three nACE structures crystallised in the P1 space group that is typical for this domain, with two molecules in the asymmetric unit. The cACE complex structures crystallised in the usual cACE $P2_12_12_1$ space group, with one molecule in the asymmetric unit.

Table 2. X-ray data collection and refinement statistics. Inner shell, overall and outer shell statistics are given in square brackets, un-bracketed and round brackets respectively.

nACE	AD011	AD012	AD013
Resolution (Å)	[73.31-10.95] (2.03-2.00)	[73.94-8.76] (1.63-1.60)	[73.97-9.31] (1.73-1.70)
Space group	P1	P1	P1
Cell dimensions (a,b,c) angles (α,β,γ)	72.8, 77.7, 81.7 Å 89.0, 64.6, 75.0°	72.9, 77.5, 82.5 Å 88.4, 64.2, 75.0°	72.9, 71.1, 82.6 Å 88.6, 64.2, 74.8°
Molecules/asymmetric unit	2	2	2
Total / Unique reflections	583,772/102,179	1,384,317/199,691	1,150,591/165,914
Completeness (%)	[99.3] 99.1 (96.2)	[98.4] 96.7 (95.4)	[99.1] 97.0 (95.8)
R_{merge}	[0.044] 0.142 (1.391)	[0.030] 0.063 (1.027)	[0.028] 0.068 (0.814)
R_{pim}	[0.019] 0.064 (0.653)	[0.012] 0.026 (0.432)	[0.011] 0.032 (0.341)
$\langle I/\sigma(I)\rangle$	[22.3] 7.2 (1.5)	[41.3] 11.6 (1.7)	[44.5] 13.3 (1.9)
$CC_{1/2}$	[0.998] 0.996 (0.418)	[0.999] 0.999 (0.461)	[0.999] 0.999 (0.720)
Multiplicity	[6.5] 5.7 (5.4)	[7.8] 6.9 (6.5)	[7.8] 6.9 (6.6)
Refinement statistics			
R_{work}/R_{free}	0.185/0.214	0.188/0.212	0.195/0.215
Rmsd in bond lengths (Å)	0.002	0.010	0.003
Rmsd in bond angles (°)	0.537	0.880	0.648
Ramachandran statistics (%)			
Favoured	98.2	98.2	98.3
Allowed	1.6	1.6	1.5
Outliers	0.2	0.2	0.2
Average B- factors (Å2)			

Protein	42.43	42.24	38.52
Ligand	58.91	58.69	59.60
Water	41.11	41.96	38.28
Number of atoms			
Protein	10066	10088	10078
Ligand	782	719	636
Water	511	798	764
PDB code	7Q24	7Q25	7Q26

cACE	AD011	AD012	AD013
Resolution (Å)	[52.03-8.21] (1.53-1.50)	[84.78-9.04] (1.68-1.65)	[66.36-8.76] (1.63-1.60)
Space group	P212121	P212121	P212121
Cell dimensions (a,b,c) angles (α,β,γ)	56.5, 85.6, 134.1 Å 90.0, 90.0, 90.0°	56.3, 84.8, 133.4 Å 90.0, 90.0, 90.0°	56.2, 84.8, 132.7 Å 90.0, 90.0, 90.0°
Molecules/asymmetric unit	1	1	1
Total / Unique reflections	2,428,701/104,713	2,533,977/77,571	2,007,770/84,046
Completeness (%)	[99.8] 100.0 (99.8)	[99.9] 100.0 (99.7)	[99.8] 99.6 (96.8)
R_{merge}	[0.054] 0.221 (2.060)	[0.056] 0.183 (4.941)	[0.045] 0.213 (1.586)
R_{pim}	[0.012] 0.047 (0.439)	[0.010] 0.032 (1.052)	[0.009] 0.044 (0.389)
$\langle I/\sigma(I) \rangle$	[34.0] 12.0 (2.7)	[50.4] 15.2 (1.2)	[46.4] 11.1 (2.4)
$CC_{1/2}$	[0.999] 0.998 (0.531)	[1.000] 0.999 (0.512)	[1.000] 0.998 (0.413)
Multiplicity	[20.6] 23.2 (22.9)	[29.5] 32.7 (22.1)	[23.7] 23.9 (17.4)
Refinement statistics			
$R_{work/}R_{free}$	0.149/0.178	0.163/0.183	0.161/0.184
Rmsd in bond lengths (Å)	0.011	0.005	0.004
Rmsd in bond angles (°)	1.049	0.821	0.756
Ramachandran statistics (%)			
Favoured	98.1	99.0	98.6
Allowed	1.9	1.0	1.2
Outliers	0.0	0.0	0.2
Average B- factors (Å2)			
Protein	17.71	27.86	19.75
Ligand	33.31	45.18	43.06

Water	30.54	35.59	29.83
Number of atoms			
Protein	4980	4787	4820
Ligand	320	269	266
Water	702	436	559
PDB code	7Q27	7Q28	7Q29

The overall structure of both ACE domains in all inhibitor-bound complexes is the typical, mostly α-helical ellipsoid and all are in the closed conformation (**Figure S2**). To allow access to the active site this ellipsoid is formed by two lobes that can open in a clam shell-like manner. The first 100 residues of the ACE domains forms part of one of these lobes serving as a flexible 'lid-like' region that can move independently from the rest of the lobe, controlling access to the active site. All the nACE and cACE inhibitor-bound structures show these features, with very little variation observed in the overall fold. This is highlighted by low RMSD values observed between all structures with a variation of 0.15 – 0.24 Å (604 Cα atoms) for nACE structures, 0.15 – 0.29 Å (578 Cα atoms) for cACE structures and a slightly higher variation of 0.90 – 0.94 Å (572 Cα atoms) between nACE and cACE structures (**Table S1)**. Examination of the mFo-DFc omit maps reveals clear, unambiguous electron density for inhibitors AD011, AD012 and AD013 bound in the S_1, S_1' and S_2' subsites, which is reflected in the final 2mFo – DFc maps (**Figure 3**).

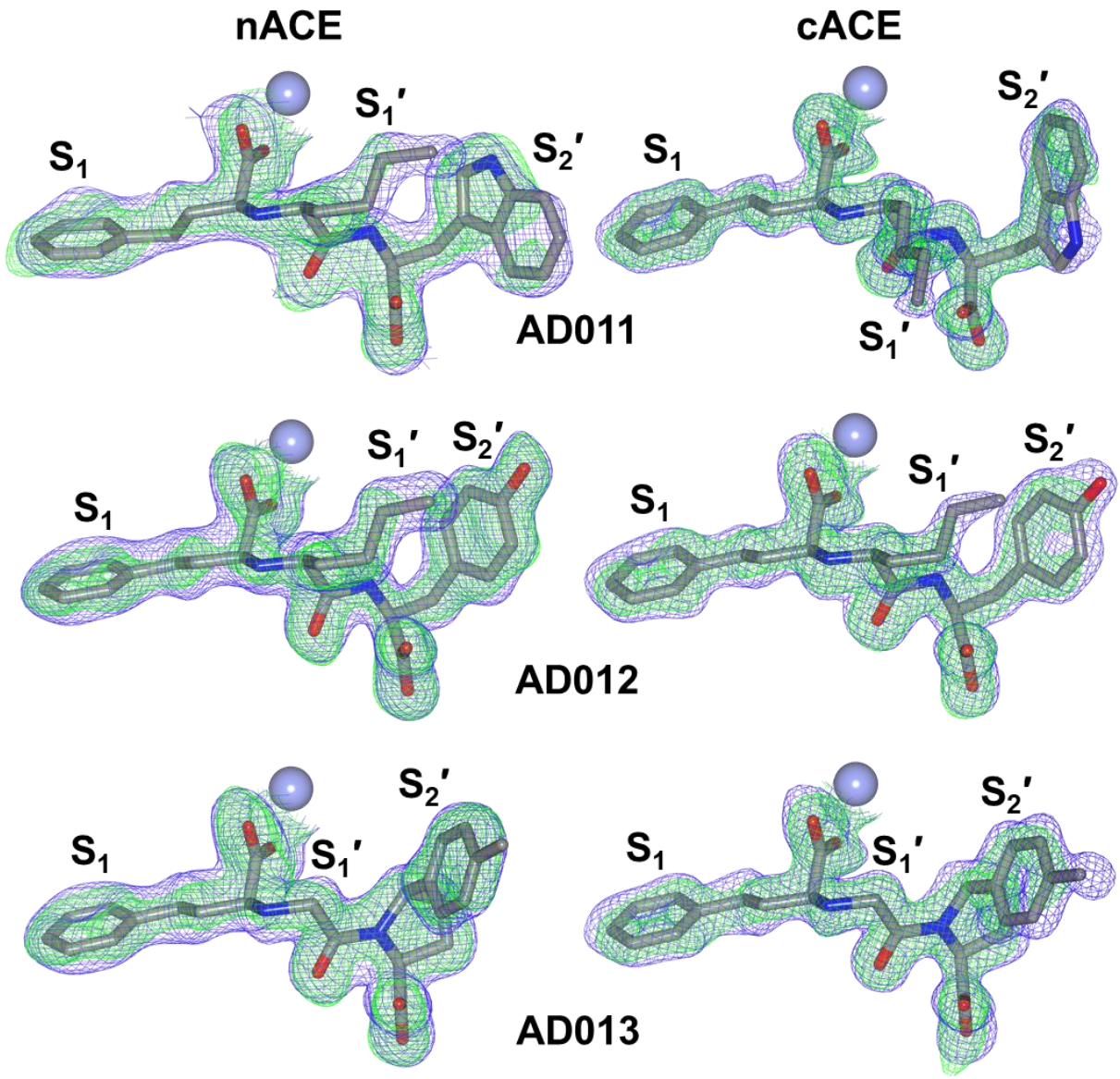

Figure 3. Inhibitors AD011, AD012 and AD013 are bound in the S_1, S_1' and S_2' subsites of nACE and cACE structures. The final 2mFo – DFc (blue, contoured at 1σ level) and the omit mFo – DFc (green, contoured at 3σ level) electron density maps for the ACE-inhibitor complex structures clearly show the inhibitors are bound in the active site occupying the S_1, S_1' and S_2' subsites. Zinc ions are depicted as lilac spheres.

Inhibitor interactions within the nACE and cACE binding sites

Comparison between the active sites of nACE and cACE show 89% identity. As the inhibitors have been designed with the same backbone and P_1 group, it is not surprising that the majority of interactions are conserved between the inhibitors and ACE domains (**Figure 4**). The completely conserved interactions within all structures include the strong coordination sphere of the zinc ion by its binding residues (nACE – His361, His365 and Glu389; cACE – His383,

His387 and Glu411) and the P_1 carboxylate group of the inhibitors. This carboxylate group also directly hydrogen bonds to Glu362/Glu384 and Tyr601/Tyr623 of nACE/cACE (this nACE/cACE nomenclature is used throughout) as well as water-mediated interactions with Ala334/Ala356 (backbone nitrogen atom), Glu363/Glu384, Glu389/Glu411, Arg500/Arg522 and Tyr501/Tyr523, with the exception that in the cACE-AD012 complex the interaction with Ala356 and Glu384 is mediated through a borate oxygen used in the crystallisation media, instead of a water molecule.

The phenylpropyl P_1 group of the inhibitors forms hydrophobic interactions with His331/His353, Ser333/Ser355, Phe490/Phe512 and Thr496/Val518 of nACE/cACE. His331/His353 and Ala332/Ala354 (backbone carbonyl oxygen atoms) interact with the inhibitor P_1' backbone amine, while the inhibitor P_1' backbone carbonyl oxygen also interacts with His331/His353 as well as His491/His513. The P_2' carboxylate group of all the inhibitors forms direct hydrogen bonds/salt bridges with the sidechains of Gln259/Gln281, Lys489/Lys511 and Tyr498/Tyr520, and a water mediated interaction with Lys489/Lys511 that are all typically observed in the peptide substrate C-terminal binding site of ACE domains. The P_2' backbone carbon atoms formed hydrophobic interactions with His491/His513 in all the complexes with all three inhibitors, but the hydrophobic interactions with Tyr501/Tyr523 were only observed for AD011 and AD012.

Unsurprisingly, the variation of the P_1' and P_2' sidechains between AD011, AD012 and AD013 results in inhibitor and domain specific interactions (**Figure 4)**. These are described in detail in the discussion below.

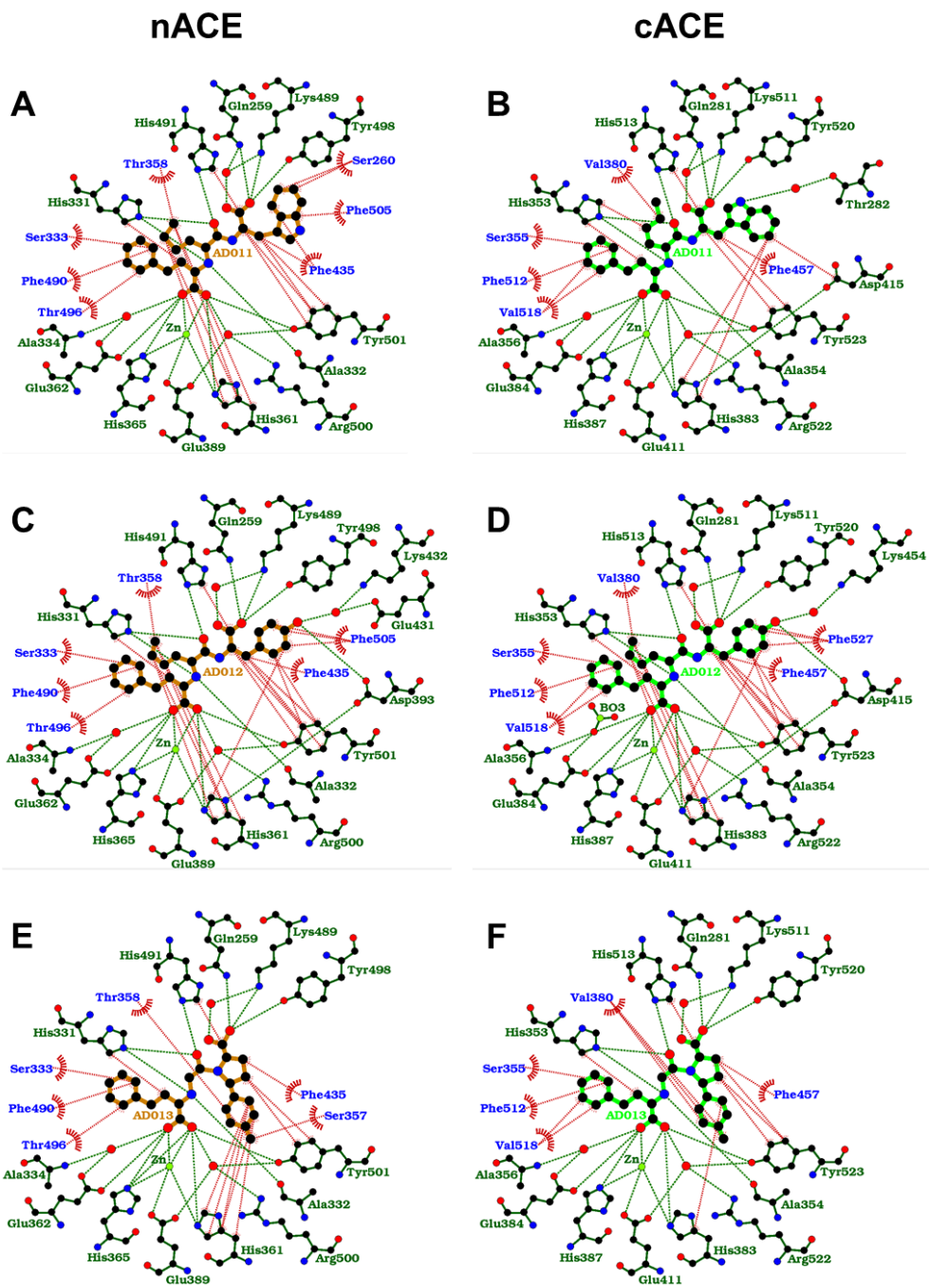

Figure 4. Ligplot representations of inhibitor binding interactions. Interaction comparison of A) nACE-AD011, B) cACE-AD011, C) nACE-AD012, D) cACE-AD012, E) nACE-AD013 and F) cACE-AD013 complexes. H-bond/electrostatic and hydrophobic interactions are shown as green and red dashed lines respectively, zinc ion and water molecules as green and red spheres, respectively. Red, semi-circular symbols depict residues solely involved in hydrophobic interactions. Ligplot representations for previously reported LisW- and Lisinopril-ACE structures are shown in Figure S3 for comparison.

Inhibitor interactions within the NEP binding site predicted by in silico docking

To date co-crystallisation studies of AD011, AD012 and AD013 with NEP were unsuccessful. Hence docking studies were used to predict NEP-inhibitor interactions. Crystal structures of NEP in complex with a range of inhibitors have been reported previously.[45-47] While the Cα backbones of these structures overlay closely, residue sidechains of Tyr693 and Phe106 which separate the S1′ and S2′ subsites as well as Arg102 and Arg110, adopt different orientations depending on the size of the bound ligand with movement of these sidechains controlling the relative sizes of the fluid S_1' and S_2' subsites. As a result, docking results need to be interpreted with caution as the NEP structure used for docking can have a significant influence on the predicted binding pose. Docking studies were carried out using the NEP-sampatrilat co-crystal structure.[49] Sampatrilat is a dual ACE and NEP inhibitor having a carboxylate zinc binding group and displaying potent NEP inhibition at low nanomolar concentrations. Predicted NEP binding poses for AD011, AD012 and AD013 are shown in Figure 5. As observed in ACE, the P_1 carboxylate coordinates with the zinc ion with the phenylpropyl P_1 group extending into the large non-prime cavity of the NEP binding site where the P_1 phenyl group forms an edge to face stacking interaction with Phe544 of NEP. The P_1 backbone amines of AD011 and AD012 form hydrogen bonds with the NEP backbone carbonyl of Ala543, while both the P_1' and P_2' backbone amines interact with Asn542 as observed for other inhibitors in NEP co-crystal structures (**Figure 5B and 5C**). The P_1' carbonyl groups of AD011 and AD012 form key bidentate interactions with Arg717. The P_2' indole methylene group and the P_2' tyrosine sidechain of AD011 and AD012 respectively, extend into the large flexible hydrophobic S_2' subsite forming hydrogen bonds with Tyr697.The tyrosine hydroxyl of AD012 forms an additional interaction with the backbone amine of Gly714. The terminal carboxylates of AD011 and AD012 are positioned at the entrance to the S_2' subsite, interacting directly with Arg102 and Arg110 as well as Asn542 in the case of AD012. Conversely, the P_2' tolyl group of AD013, constrained by the pyrrolidine ring, does not appear to be able to adopt a conformation for favourable binding in the S_2' subsite. Instead, the predicted binding pose shows the tolyl group positioned in the S_1' subsite resulting in unfavourable van der Waals interactions with Arg717 (**Figure 5D**). This binding pose is likely to be facilitated by the increased flexibility resulting from the lack of a P_1' sidechain. The unfavourable binding in the S_1' subsite and the absence of interactions in the S_2' subsite provides an explanation for the lack of NEP inhibitory activity observed for this compound.

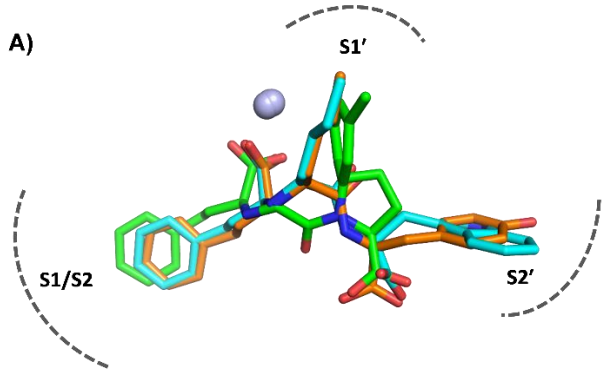

B) NEP- AD011

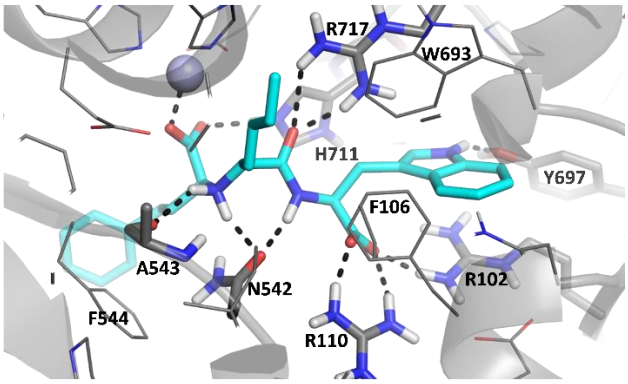

C) NEP - AD012

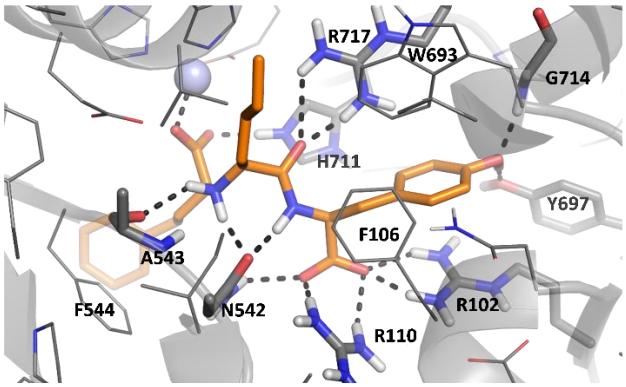

D) NEP - AD013

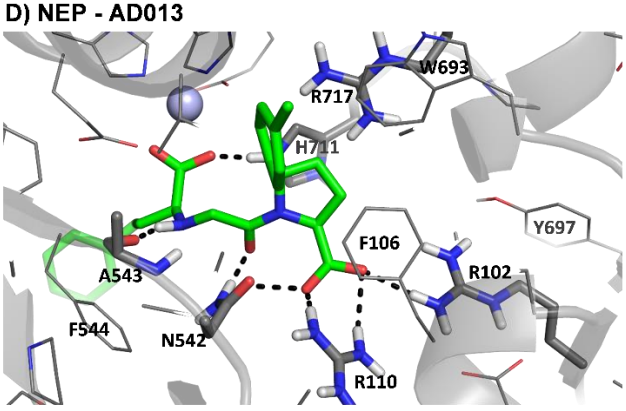

Figure 5. In silico docking predicts protein-inhibitor interaction of carboxy-3-phenylpropyl dipeptide inhibitors within the NEP active site.

A) Overlay of inhibitors AD011 (cyan), AD012 (orange) and AD013 (light green) docked into the binding site of the NEP-sampatrilat co-crystal structure (PDB 6XVP). Predicted protein-inhibitor interactions for B) AD011, C) AD012 and D) AD013 within the NEP active site. Zinc ions are depicted as lilac spheres. Polar interactions are depicted as dotted lines, with key interacting residues shown as sticks.

DISCUSSION

LisW is a potent cACEi, displaying two orders of magnitude C-selectivity, but does not inhibit NEP (K_i of >150 μM). NEP has a hydrophobic S_1' subsite favouring ligands with long and/or bulky hydrophobic P_1' groups.[45, 47] To match this preference the amino group of the LisW P_1' lysine was removed in AD011, dramatically increasing its potency for NEP from a K_i of >150 μM to 19 μM. This change in the P_1' group caused a small increase in the K_i for nACE, from 1.7 to 3.79 μM, but decreased affinity for cACE, with the K_i increasing from 0.009 to 0.10 μM. Therefore, while this modification of LisW to form AD011 had the desired effect of increasing its affinity for NEP, it reduced the C-selectivity from 189- to 37-fold. However, the resultant level of C-selectivity still might be sufficient physiologically if the affinity for NEP could be further improved. The results observed for AD011 are consistent with previous site-directed mutagenesis studies probing the interactions conferring C-selectivity for other related inhibitors, suggesting that moderate selectivity can be achieved by incorporation of a tryptophan residue at the P_2' position, but additional domain-specific interactions need to be exploited to obtain higher levels of selectivity. For previously reported matched inhibitor pairs (lisinopril and LisW, and keto-ACE inhibitors kAP and kAW), where a proline at the P_2' was substituted for tryptophan, an increase of ~40 to 50 fold C-selectivity was observed.[33] The higher overall selectivity observed for LisW (C-selectivity factor ~189) can be attributed to the presence of the P_1' lysine (also present in lisinopril with a C-selectivity factor of ~4) in combination with the P_2' tryptophan group (**Table 1**). In the case of keto-ACE inhibitors, the proline derivative kAP showed a C-selectivity factor of 30 (**Figure S4**). Site directed mutagenesis studies, where cACE-specific residues were mutated to the corresponding nACE residues, showed that the selectivity of kAP could be attributed to interactions of the P_1 and P_2 phenyl rings with unique residues in the non-prime subsites. The substitution of the P_2' proline for a tryptophan in kAW increased the C-selectivity to 1255 (41-fold relative to kAP).

The recently published crystal structure of NEP in complex with the high-affinity inhibitor sampatrilat (IC_{50} of 8 nM) showed that a P_2' tyrosine group is well accommodated in the S_2' subsite, forming multiple hydrophobic interactions with Phe106, Arg109, Arg110 and Trp693, as well as a hydrogen bond with Asp107.[46] Changing the P_2' tryptophan group of AD011 to a tyrosine to give AD012 further increased the affinity for NEP (K_i of 0.6 μM). This also increased its affinity for cACE (K_i of 0.035 μM) compared to AD011, but a greater increase was observed for nACE (K_i of 0.12 μM), resulting in a decrease of the C-selectivity factor to 3.5. Further probing, by replacing the hydroxyl with other functionality, would be needed to determine whether improved C-selectivity could be achieved. For example, it would be interesting to test the effect of removing this hydroxyl group on C-selectivity and NEP potency. A third keto-ACE derivative, kAF, with a phenylalanine at the P_2' position, displayed >600-fold C-selectivity, increasing the C-selectivity of the matched pair kAP > 20-fold (**Figure S4).**[33] kAF (phenylalanine at the P_2') and kAW (tryptophan at the P_2') displayed similar affinity for cACE, suggesting that a phenylalanine may offer an alternative at the P_2' position.

An SAR study using a series of 2-mercapto-3-phenylpropanoyl compounds with a P_1' glycine and P_2' 5-phenylproline-based groups gave high affinity inhibition of both rabbit NEP and tACE (nACE inhibitory potency was not determined).[5] Creating the 1-carboxy-3-phenylpropyl compound with these P_1' and P_2' C-terminal groups to give compound AD013 resulted in a significant reduction in affinity for NEP (K_i of >50 μM) in line with docking studies showing an unfavourable binding pose in NEP. This is likely due to i) the lack of a P_1' sidechain resulting in binding to only one of the NEP prime subsites being possible and ii) in contrast to the 2-mercapto-3-phenylpropanoyl in omapatrilat and the previously reported 5-phenylproline compounds, the 1-carboxy-3-phenylpropyl in AD013 is not tolerated in the S_1' position of NEP. The latter is possibly because the carboxy zinc coordination does not allow for optimal binding of the P_2' group in this binding orientation. This is consistent with the observation that many current-generation selective ACE inhibitors in the clinic, presumably displaying poor affinity for NEP, contain a 1-carboxy-3-phenylpropyl N-terminal group and lack a long/bulky P_1' sidechain for binding to the NEP S_1' subsite, typically with an alanine at the P_1' position. Although AD013 has a similar nACE affinity (K_i of 3.4 μM) to AD011, it only has a moderate C-selectivity factor of 8 (K_i for cACE of 0.44 μM), and the structural work indicates that further modification of the phenylpropyl and/or zinc binding group may be required to improve NEP

binding, and to allow for the alternative binding orientation likely required for potent NEP inhibition.

Although none of the compounds in the present study met the requirements of a dual cACEi/NEPi, a detailed analysis of the inhibitor binding interactions in the co-crystal structures provides valuable insights to drive the design of inhibitors with improved C-selectivity and NEP potency. The enzyme inhibition data (**Table 1**) shows the C-selectivity factors for lisinopril, LisW, AD011, AD012 and AD013. Overlays of each inhibitor in complex with nACE and cACE (**Figure 6 and 7**) and comparison of the interactions in each ACE domain (**Figure 4 and Figure S3**) can give insights into the observed variation in C-selectivity. In addition, comparison of predicted NEP-inhibitor binding poses with those observed for other NEP inhibitors in co-crystal structures can shed light on the factors driving NEP potency.

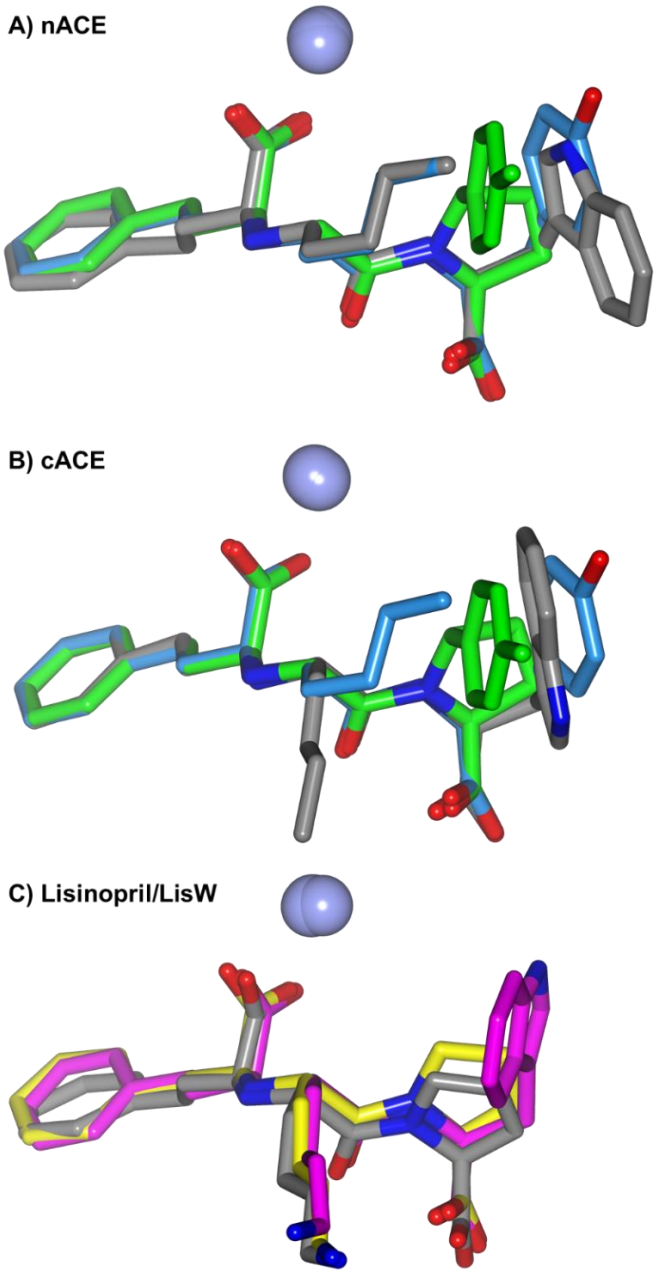

Figure 6. Comparison of carboxy-3-phenylpropyl dipeptide inhibitors binding within each ACE domain. Overlay of AD011 (grey), AD012 (light blue) and AD013 (light green) inhibitors bound to A) nACE and B) cACE. C) Overlay of LisW-cACE (magenta, PDB 3L3N), lisinopril-nACE (grey, PDB 2C6N) and lisinopril-cACE (yellow, PDB 1O86) complex structures. Zinc ions are depicted as lilac spheres

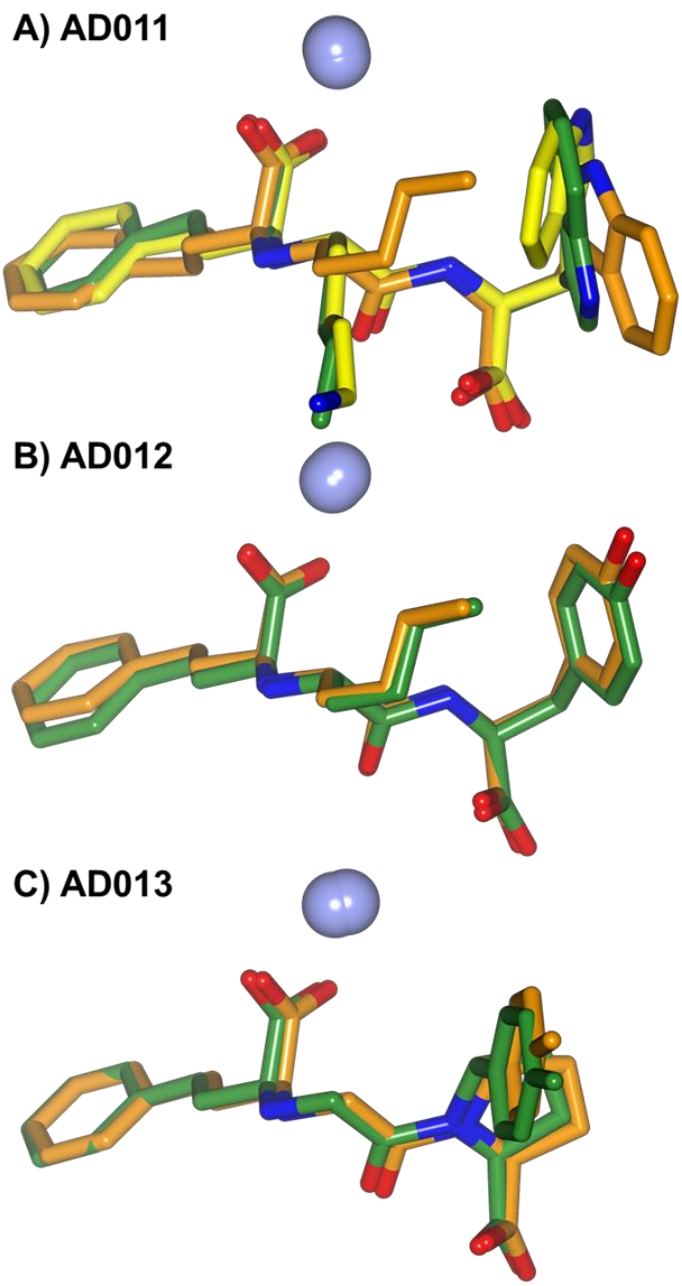

Figure 7. Comparison of carboxy-3-phenylpropyl dipeptide inhibitors binding between ACE domains. Overlay of nACE (light orange) and cACE (green) structures in complex with A) AD011, B) AD012 and C) AD013 inhibitors. Zinc ions are depicted as lilac spheres. Overlay of LisW-cACE (PDB 3L3N, yellow) is included in (A) for comparison.

All these inhibitors bind in the same orientation with the conserved P_1 3-phenylpropyl group extending into the S_1 subsite, overlaying closely for all inhibitors in both domains, as do the zinc binding carboxylates, the main chain atoms of the P_1' and P_2' groups and the P_2'

carboxylate (**Figure 6 and 7**). The only notable domain-dependent difference in binding interactions in the S_1 subsite is a stronger double hydrophobic interaction between the cACE specific residue Val518 and the P_1 phenyl ring, compared to a single interaction from the less hydrophobic Thr496 of nACE at the equivalent position. While it is possible that this contributes to the observed C-selectivity, mutation of Val518 to the corresponding nACE residue Thr496 did not significantly alter the K_i of lisinopril or LisW.[39] The majority of inhibitor- and domain-dependent differences in binding interactions were observed within the S_1' and S_2' subsites. These are discussed in more detail in the sections below.

Comparison of inhibitor binding within nACE S_1' and S_2' subsites

In nACE the P_1' *n*-butyl groups of compounds AD011 and AD012 adopt nearly identical conformations extending towards the S_2' subsite of nACE and forming a series of hydrophobic interactions with Thr358 and His361 (**Figures 4 and 6A**). The P_2' indole methylene group of AD011 forms extensive hydrophobic interactions with Ser260, Phe435, Tyr501 and Phe505 as does the P_2' tyrosine phenyl of AD012. The 30-fold difference in affinity for nACE between the two compounds is likely due to the tyrosine hydroxy group of AD012 additionally forming a direct hydrogen bond with Asp393 and water-mediated interactions with Glu431 and Lys432.

Compound AD013 lacks a P_1' sidechain to interact with nACE in the S_1' subsite and has the P_2' tolyl group constrained by the pyrrolidine ring preventing the tolyl group from aligning with the indole or phenol of AD011 and AD012. The position of the P_2' tolyl group is significantly closer to the S_1' subsite and would enter a steric clash with a with a P_1' sidechain adopting a AD011/AD012 conformation, thereby preventing an overall favourable binding conformation in the nACE complex. However, it does form extensive hydrophobic interactions where its pyrrolidine ring stacks over Tyr501, the phenyl ring forms an edge-to-π face stacking with His361 and there are additional hydrophobic interactions with Ser357 and Phe435. Despite significantly different interactions in the S_1' and S_2' subsites, AD011 and AD013 have similar affinities for nACE. Overall, it is clear that a tyrosine C-terminal group for these inhibitors is beneficial for nACE affinity with AD012 displaying the lowest nACE K_i.

Comparison of inhibitor binding within cACE S_1' and S_2' subsites

In cACE the P_1' *n*-butyl sidechains of AD011 and AD012 adopt different conformations resulting in variation of the interactions in the cACE S_1' subsite (**Figure 6B**). There are two hydrophobic interactions with His353 and Val380 in the AD011-cACE complex, but a more extensive hydrophobic network was observed with Val380 and His383 in the AD012-cACE complex (**Figure 4**). This change in the P_1' *n*-butyl sidechain orientation is accompanied by a shift in orientation of the P_2' indole and phenol groups of AD011 and AD012. The indole of AD011 is shifted a little closer to the S_1' subsite than the phenol of AD012, which would cause a steric clash if the *n*-butyl sidechain adopted the same orientation observed in the AD011-cACE complex. The P_2' phenol of AD012 has direct and water-mediated hydrogen bonds with Asp415 and Lys454, respectively, as well as a network of hydrophobic interactions with Phe457, Tyr523 and Phe527. These binding interactions are more extensive than those observed for the P_2' indole of AD011 and may explain the slightly higher affinity of cACE for AD012 than AD011.

Due to the structure of the P_2' arylpyrrolidine of AD013, it occupies a region of the cACE S_2' subsite that is closer to the S_1' subsite than the P_2' indole and phenol groups of AD011 and AD012, where it forms a hydrophobic network with Val380, His383, Phe457 and Tyr523. Compound AD013 is the weakest of the three inhibitors for cACE, which could be explained by the lack of sidechain interactions in the S_1' subsite. It is also possible that, while the hydrophobic interactions in the S_2' subsite are extensive, they may not be optimal, and unlike the cACE AD011 and AD012 complexes, there are no hydrogen bonds formed.

Comparison of inhibitor binding between nACE and cACE.

While there is no structure of nACE in complex with LisW in the PDB, there are LisW-cACE, lisinopril-nACE and lisinopril-cACE structures available,[39, 50, 51] which along with the structures presented here, allow for a detailed comparison of how binding interactions relate to inhibition data.

The S_1' and S_2' subsites of ACE domains are not well-defined pockets but are fairly open regions allowing for flexibility of binding for the P_1' and P_2' groups. This is highlighted by the overlays of AD011 and AD012 derived from the two ACE domain structures (**Figures 7A and**

B), which show a significant difference in the orientation of the P_1' sidechain of AD011-cACE complex compared to the other three structures. This P_1' conformation in AD011-cACE is the same as that observed for lysine P_1' sidechains in the lisinopril and LisW ACE structures (**Figure 6C**). The P_1' amino groups of lisinopril/LisW make a series of longer and water-mediated hydrogen bonds with Glu162 and Asp377 in cACE (the resolution of the lisinopril nACE structure is too low to show water molecules, but Gln355 and Thr358 are close enough for water-mediated interactions), and the alkyl chains engage in hydrophobic interactions in all structures (**Figure S3**). Removal of the LisW amine with AD011 prevents the electrostatic interactions with Glu162 and Asp377 in cACE, which is likely to contribute to the lower observed K_i. The lysine sidechains of lisinopril and LisW therefore adopt a different orientation relative to the *n*-butyl chains of AD012 in both nACE and cACE, as well as AD011 in nACE, which are orientated more towards the S_2' subsite. The lysine sidechain of lisinopril would be unable to adopt this alternate conformation as it would be sterically hindered by the P_2' proline ring in both nACE and cACE. LisW has only a single additional P_1' amino group than AD011 with the AD011-nACE structure showing space for this amino group. Therefore, the lysine sidechain of LisW could adopt either conformation in the nACE, but there is no structure available to observe which is favoured. When bound to nACE, the amino group of LisW has only a small beneficial effect on nACE potency when compared to AD011 (**Table 1**). This is in line with improved enthalpic binding, due to the likely hydrogen bonding network surrounding the amino group being offset by an entropic penalty of bringing the charged amine from the water environment to the enzyme biding site. Arg350 of nACE (Thr372 in cACE) is typically orientated with the sidechain pointing inside the structure such that the guanidino group forms part of the S_1' subsite surface. However, in the lisinopril-nACE structure this arginine rotates to avoid positive charge clashes with the P_1' amino group of lisinopril such that the sidechain points out to the surface of the protein at the lip of the clam-shell opening. Not only do the P_1' groups of AD011 and AD012 not contain an amino group, but their orientation leaves the region around Arg350 clear and the sidechain of Arg350 adopts its typical conformation, with the guanidino group orientated towards the S_1' subsite.

The structures of ACE in complex with AD011 and LisW also show flexibility in binding orientation of the P_2' group, where the conformation of both the LisW and AD011 P_2' indole groups in the cACE structures would sterically hinder the P_1' sidechains from adopting the

alternate conformation seen in the AD011-nACE complex. The indole P_2' groups overlay in the same region of the S_2' pocket in the cACE structures, but have flipped orientations. This alters the binding within the subsite where the AD011 indole forms a water-mediated hydrogen bond with Thr282 as well as hydrophobic interactions with His383, Asp415 and Phe457 (**Figure 4A**), compared to the LisW tryptophan forming a direct hydrogen bond with Asp415 and a more extensive hydrophobic network with Val380, Phe457, Tyr523, Phe527 and Tyr523 (**Figure S3**). Given the identical residues and environment, it is not immediately clear why the tryptophan sidechains of LisW and AD011 are flipped when comparing the two cACE complexes. Closer examination shows that, while the *n*-butyl of AD011 adopts a similar orientation to the P_1' lysine sidechain of LisW, they do not overlay exactly. Instead, interactions of the LisW lysine amino group pulls the lysine carbon atoms a little closer to the S_2' subsite relative to the *n*-butyl of AD011, perhaps sufficiently to flip the indole. The orientation of the indole ring in the S_2' subsite observed for AD011 has previously been observed for C-selective ACE inhibitors kAW and RXPA380.[33] Therefore, even though the only difference between AD011 and LisW is the P_1' amine group, it is a combination of differences in interactions in both the S_1' and S_2' subsites of cACE that account for the higher affinity of LisW.

The rotation of the P_2' indole of AD011 in the nACE complex is closer to that of LisW-cACE than AD011-cACE, but it is positioned further away from the S_1' subsite. This appears to be caused by two non-conserved residues (**Figure 8A**). Firstly, Ser260 of nACE is replaced by Thr282 in cACE, where the CG2 atom of Thr282 would clash (with a less than allowable 2.70 Å van der Waals contact) with the indole of AD011 if the orientation observed in nACE was maintained. Secondly, Gly439 of nACE is replaced by Ser461 in cACE. While these residues are not adjacent to the S_2' subsite, the sidechain of Ser461 causes small shifts in the sidechains of Phe457 and Phe527 in cACE compared to those in nACE (Phe435 and Phe505). These residues engage in hydrophobic interactions with the P_2' indole of AD011, pushing the sidechain a little closer to the S_1' subsite in cACE. While there also appears to be a consistent similar shift of the P_2' sidechain of AD012 and AD013, it is much smaller and therefore could just be representative of general protein flexibility. The binding orientation and interactions observed for AD011 in cACE are more favourable than those observed in nACE, as highlighted by the C-selectivity factor of 37.

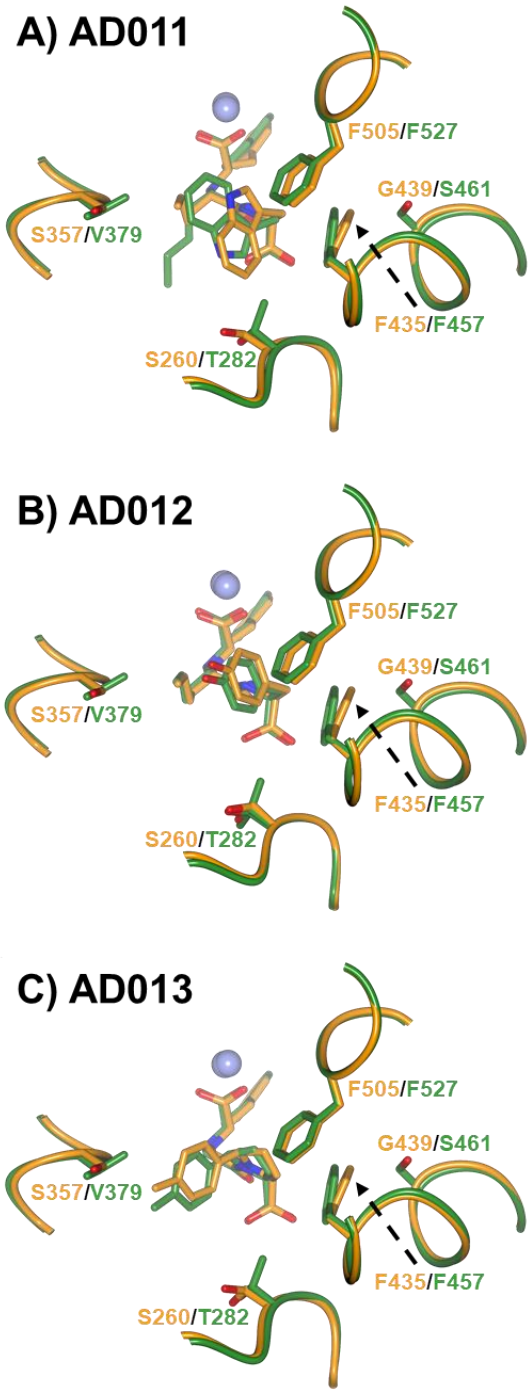

Figure 8. Residue differences between nACE and cACE that affect inhibitor binding orientation. Overlay of nACE (light orange) and cACE (green) structures in complex with A) AD011, B) AD012 and C) AD013 inhibitors. Zinc ions are depicted as lilac spheres.

In contrast, the C-selectivity for AD012 is low at 3.5-fold. The overlay of the nACE- and cACE-AD012 complexes (**Figure 7B and 8B**) shows an almost identical binding orientation.

With the P_2' tyrosine of AD012 in cACE occupying almost the same region as observed for the P_2' groups of AD011 and AD012 in nACE, it allows space for the P_1' *n*-butyl of AD012 to adopt the alternate conformation closer to the S_2' subsite. The P_2' tyrosine hydroxyl of AD012 forms a water-mediated interaction with a lysine residue in both of the nACE and cACE complexes (Lys432/Lys454). The greater increase in nACE binding potency relative to cACE for this tyrosine analogue might be due to the bridging water molecule being further held in place by the carboxylate of Glu431 in nACE (corresponding to Asp453 in cACE). Based on these observations, it is possible that if the P_2' tryptophan of LisW was replaced with a tyrosine, then a higher affinity nACE inhibitor would be achieved. In addition, the data from AD012 shows that although a P_2' tyrosine is favourable for NEP binding, it should be avoided for the design of a dual cACEi/NEPi due to the increase in nACE affinity.

Like AD012, the inhibitor AD013 overlays closely in the nACE and cACE complexes, with only a slight difference observed for the P_2' group mentioned above (**Figure 7C and 8C**). Val379 of cACE is bulkier than the equivalent Ser357 of nACE, which is consistent with the small shift. However, Val379 and Val380 (Thr358 in nACE) are also likely to provide a more beneficial hydrophobic environment for the P_2' group of AD013, which could also contribute to the slightly higher C-selectivity observed for AD013 relative to AD012.

Comparison of NEP docking poses with other inhibitors in NEP co-crystal structures

High-resolution crystal structures of NEP in complex with a range of potent NEP inhibitors have been reported, providing insight into key interactions driving NEP potency. Inhibitor potency is primarily driven by interactions with residues lining the S_1' and S_2' subsites, as there are no distinct subsites in the large non-prime cavity of the NEP binding site limiting the potential for interactions with the P_1 group. Although in the NEP docking structures presented here, the P_1 phenyl ring of all three compounds did form an edge to face stacking interaction with Phe544 of NEP, so this could be an area to further explore to increase potency. The S_1' is hydrophobic with high specificity for hydrophobic or aromatic groups. The large S_2' is less specific than the S_1', accommodating a range of different moieties in distinct binding orientations. In comparison to inhibitor binding in ACE where inhibitors typically bind in a linear conformation, NEP inhibitors are typically required to adopt a bent conformation due to

the differences in the relative positions of the subsites in these two proteins[46], as observed in the docking complexes of AD011 and AD012 (**Figure 5 and 9**).

Comparison of the predicted binding pose of AD011 with the binding pose observed for the potent NEP inhibitor phosphoramidon in a NEP co-crystal structure[45] revealed differences in the binding orientations of the shared P_2' tryptophan in the S_2' subsite (**Figure 9a**). NEP-inhibitor co-crystal structures reveal that the size of the group binding to the S_1' subsite affects the conformation of the residue sidechains separating the S_1' and S_2' subsites, influencing the binding orientation of the P_2' group. When the NEP-phosphoramidon structure (PDB 1DMT) was used for docking instead of the NEP-sampatrilat structure (PDB 6XVP) the predicted binding orientation of the tryptophan was very similar to that of phosphoramidon (**Figure 9a**). Despite this similarity, the original docking pose in the NEP-sampatrilat was predicted to be more energetically favoured. Similarly, Figure 9b shows an overlay of the predicted NEP binding pose for AD012, the most potent of the three carboxy-3-phenylpropyl dipeptides, and sampatrilat. In this case, even though the same structure was used for docking, the shared P_2' tyrosine residues adopt different conformations in the S_2' subsite. These examples highlight the challenges using static NEP structures to design new inhibitors. In contrast, AD013 was predicted to bind to NEP with an unfavourable binding pose consistent with a lack of NEP inhibitory activity (K_i > 50 µM).

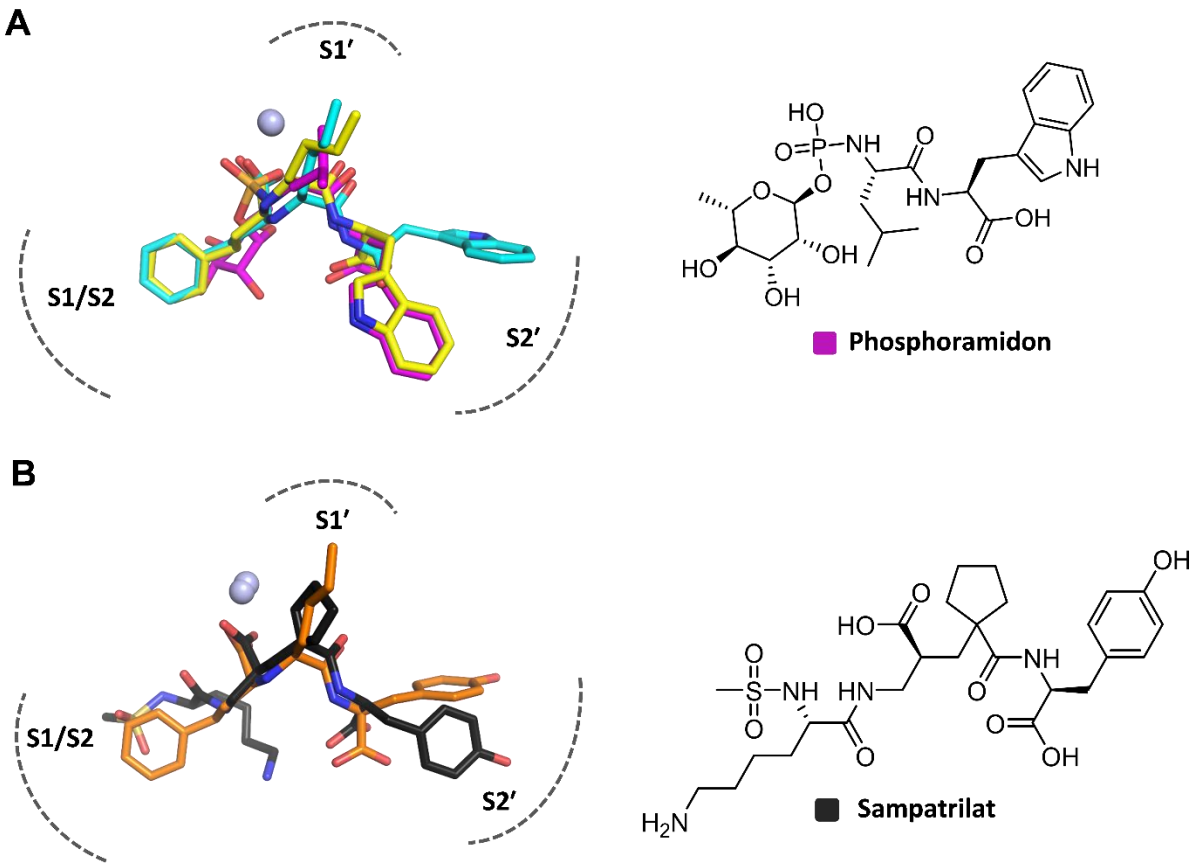

Figure 9. Comparison of predicted binding poses for carboxy-3-phenylpropyl dipeptides with binding poses of known inhibitors co-crystallised with NEP.

A) Overlay of phosphoramidon (magenta) co-crystallised with NEP (PDB 1DMT) and AD011 docked into NEP PDB structures 6XVP (cyan) and 1DMT (yellow). B) Overlay of sampatrilat (black) co-crystallised with NEP (PDB 6XVP) and AD012 (orange) docked into NEP (PDB 6XVP). Zinc ions are depicted as lilac sphere and subsites are indicated by dashed lines.

CONCLUSION

In summary, inhibition data and high-resolution inhibitor-bound structures for LisW analogues AD011, AD012 and AD013, provide new insights into the factors driving C-selectivity and NEP potency, contributing to the design of dual cACE/NEP inhibitors. As predicted, removing the P_1' amine in LisW (AD011) improved the inhibitory potency for NEP, but this compound still showed poor NEP affinity relative to both nACE and cACE affinity, and removal of the amine resulted in a moderate reduction in C-selectivity (5-fold).

Changing the AD011 P_2' tryptophan group to a tyrosine (AD012), further enhanced binding to NEP, but the C-selectivity of AD012 was poor, due to strong binding of the tyrosine in the

nACE S_2' subsite. Overall, this suggests that directed analogue work focused on exploring different combinations of functionalities at the P_1' and P_2' positions to increase C-selectivity and NEP potency is warranted. While previous work on domain selective inhibitors has focused on interactions in the S_2' and/or non-prime subsites, this work highlights the important role of the P_1' sidechain for C-selectivity and the fluidity between the S_1' and S_2' subsites. Similarly to ACE, there is also interplay between the NEP S_1' and the S_2' subsites. Inhibitor-bound NEP co-crystal structures show that a bulky group in the S_2' pocket causes the sidechain of Trp682 to swing towards the S_1' pocket, constricting this pocket. Consequently, a bulky group can be accommodated in either the NEP S_1' or S_2' subsites, but bulky groups at both these positions may be detrimental to inhibitor binding.

Compound AD013 displayed reduced affinity for NEP and cACE relative to previously reported 2-mercapto-3-phenylpropanoyl analogues with the same P_1' and P_2' groups. It is interesting to note that small molecules can bind in different orientations in NEP and ACE, as demonstrated by omapatrilat where the phenyl ring resides in the S_1 subsite of nACE and cACE[43] and in the S_1' subsite of NEP.[46] For inhibitors lacking P_1' sidechains suitable for binding to the NEP S_1' subsite, it appears that inhibitors with a 2-mercapto-3-phenylpropanoyl N-terminus may be better able to adopt this alternative binding orientation in NEP.

To our knowledge, this is the first reported structure-guided effort towards the design of dual cACE/NEP inhibitors. Understanding inhibitor and domain specific interactions and interplay between subsites can inform further analogue work to probe cACE versus nACE selectivity and the requirements for dual cACE/NEP inhibition. We have recently shown that the dual ACE and NEP inhibitor sampatrilat displays 12-fold C-selectivity, which can be attributed to the non-prime region of the molecule.[46, 49] SAR exploration at the P_1 and P_2 positions to exploit domain specific interactions in the S_1/S_2 subsites of cACE may also serve as an additional strategy for improving C-selectivity without disrupting NEP binding.

EXPERIMENTAL SECTION

Chemistry. All commercial reagents were purchased from Sigma-Aldrich, Combi-Blocks, Enamine, or Fluorochem and were used without further purification. Solvents were used as received unless otherwise stated. In general, the course of reactions was followed by TLC or liquid chromatography/mass spectroscopy (LC/MS). Flash column chromatography was performed using a Biotage Isolera Flash Chromatography system with SiO_2 60 (particle size 0.040−0.055 mm, 230−400 mesh). Purity of all final derivatives for biological testing was confirmed to be >95% as determined using either an Agilent 1260 HPLC/Agilent 1200 MS system with an Agilent 6120 quadrupole (single) mass spectrometer, equipped with APCI and ESI multimode ionization source while using an XBrigde C8 column, a mobile phase B of 0.1% trifluoroacetic acid in acetonitrile, a mobile phase A of 0.1% trifluoracetic acid in water, with flow rate of 0.5 mL/min, detector diode array (DAD) in a 95:5 gradient over 6 minutes. GC-MS were determined on an Agilent 7697A instrument with a 30 m Agilent 19091J-413 column over a 10 min temperature gradient of 40-325 °C using helium as the carrier with EI ionization of 70 eV. ^{1}H and ^{13}C NMR spectra were recorded on a Bruker spectrometer at 400 and 75.5 MHz, respectively. Chemical shifts (δ) are given in ppm downfield from TMS as the internal standard. Coupling constants, *J*, are recorded in hertz (Hz).

Synthesis of (*S*)-2-(((*S*)-1-ethoxy-1-oxo-4-phenylbutan-2-yl)amino)hexanoic acid (3): A solution of *tert*-butyl (*S*)-2-aminohexanoate (4.15 g, 22.1 mmol), K_2CO_3 (3.82 g, 27.7 mmol) and ethyl (*R*)-2-bromo-4-phenylbutanoate[52] (5 g, 18.5 mmol) in acetonitrile (50 ml) was heated at 120 °C in a microwave oven for 2 h. (Note: the reaction was done in five batches, 10 ml each). The batches were combined, and solids were removed by filtration with rinsing through twice with 50 ml EtOAc. The combined filtrate was concentrated to afford crude material that was purified by column chromatography to afford 1.5 g (21% yield) of a light brown solid. The solid was dissolved in trifluoroacetic acid (15 ml) with stirring at 0 °C for 10 min. The reaction mixture was concentrated to give the title compound as an orange gummy solid. The resulting residue was taken to the next step as such without any further purification. GC-MS: $(M+H)^+$: 270.0, 272.0; NMR ($CDCl_3$) δ 7.2-7.33 (m, 3H), 7.3-7.4 (m, 2H), 4.1-4.3 (m, 3H), 2.7-2.9 (m, 2H), 2.2-2.4 (m, 2H), 1.95-2.15 (m, 2H), 1.3 (t, *J* = 7 Hz, 3H). Yield: 1.5 g; 21%.

Synthesis of (*S*)-2-(((*S*)-1-(((*S*)-1-carboxy-2-(1H-indol-3-yl)ethyl)amino)-1-oxohexan-2-yl)amino)-4-phenylbutanoic acid (4, AD011): A solution of propanephosphonic acid anhydride (50% in EtOAc) (2.22 ml, 3.5 mmol) was added to a solution of the preceding compound 3 (0.75 g, 2.33 mmol), L-tryptophan methyl ester hydrochloride (0.773 g, 3.03 mmol) and triethylamine (0.707 g, 7.0 mmol) in THF (20 ml) at 0°C. The mixture was warmed to rt over 25 min at 0°C, before being quenched with ice-cold water and extracted twice with EtOAc. The combined organic layer was dried over Na_2SO_4 and concentrated to afford the title compound as a brown gummy solid that was dissolved in THF (5 ml) and water (5 ml) at 0°C before adding LiOH (0.161 g, 4.0 mmol). The reaction mixture was warmed to rt before being dilutedwith water and extracted twice with EtOAc. The combined organic layer was dried over Na_2SO_4 and concentrated to give crude product that was purified by reverse phase HPLC (water/acetonitrile gradient with 0.1% TFA method) to afford the title compound as a white solid. Yield: 0.085 g; 2.4%. LCMS: $(M+H)^+$: 480.3; ^{1}H NMR (d^6-DMSO) δ 10.9 (s, 1H), 7.9 (d, *J* = 8 Hz, 1H), 7.5 (d, *J* = 8 Hz, 1H), 7.3 (d, *J* = 8 Hz, 1H), 7.2-7.25 (m, 2H), 7.1-7.2 (m, 2H), 7.05 (t, *J* = 8 Hz, 1H), 6.95 (t, *J* = 8 Hz, 1H), 4.55 (q, *J* = 6 Hz, 1H), 3.1-3.3 (m, 2H), 3.0 (t, *J* = 6 Hz, 1H), 2.95 (t, *J* = 6 Hz, 1H), 1.65-1.8 (m, 2H), 1.35-1.55 (m, 2H), 1.15-1.3 (m, 4H), 0.7 (m, 3H). ^{13}C NMR (d^6-DMSO) δ 175.7, 173.7, 173.3, 142.2, 136.5, 128.7, 128.6, 127.8, 126.1, 124.0, 121.3, 118.7, 111.8, 109.9, 61.8, 60.3, 52.7, 33.4, 32.0, 27.6, 22.5, 14.2.

Synthesis of (*S*)-2-(((*S*)-1-(((*S*)-1-carboxy-2-(4-hydroxyphenyl)ethyl)amino)-1-oxohexan-2-yl)amino)-4-phenylbutanoic acid (5, AD012): A solution of propanephosphonic acid anhydride (50% in EtOAc) (2.22 ml, 3.5 mmol) was added to a solution of (*S*)-2-(((*S*)-1-ethoxy-1-oxo-4-phenylbutan-2-yl)amino)hexanoic acid **3** (0.75 g, 2.33 mmol), L-tyrosine methyl ester hydrochloride (0.702 g, 3.03 mmol) and triethylamine (0.707 g, 7.0 mmol) in THF (20 ml) at 0°C. The mixture was warmed to rt over 25 min at 0°C, before being quenched with ice-cold water and extracted twice with EtOAc. The combined organic layer was dried over Na_2SO_4 and concentrated to afford the title compound as a brown gummy solid. The material was dissolved in THF (5 ml) and water (5 ml) at 0°C, and LiOH (0.168 g, 4.0 mmol) was added. After warming to rt, the reaction mixture was diluted with water and extracted twice with EtOAc. The combined organic layer was dried over Na_2SO_4 and concentrated to give crude product which was purified by reverse phase HPLC (water/acetonitrile gradient with 0.1% TFA method) to afford the title compound as a white solid. Yield: 0.085 g; 8%. LCMS: $(M+H)^+$:

497.2; ^{1}H NMR (d^{6}-DMSO) δ 12.5 (br. s, 1H), 10.9 (s, 1H), 8.2 (d, *J* = 7 Hz, 1H), 8.15 (d, *J* = 7 Hz, 1H), 7.7 (br. s, 2H), 7.55 (d, *J* = 8 Hz, 1H), 7.15-7.2 (m, 4H), 7.05 (t, *J* = 8 Hz, 1H), 6.95-7.05 (m, 1H), 4.45 (q, *J* = 6 Hz, 1H), 4.35 (q, *J* = 7 Hz, 1H), 3.7 (q, *J* = 7 Hz, 1H), 3.1-3.2 (m, 2H), 3.0 (dd, *J* = 15, 8 Hz, 1H), 2.65-2.8 (m, 4H), 1.6-1.7 (m, 1H), 1.45-1.55 (m, 3H), 1.25-1.35 (m, 3H). ^{13}C NMR (d^{6}-DMSO) δ 173.6, 172.2, 171.7, 139.1, 136.5, 129.5, 129.2, 129.6, 126.6, 124.1, 121.4, 118.8, 118.6, 111.8, 110.1, 53.4, 52.4, 42.8, 41.4, 39.2, 32.3, 27.5, 27.2, 22.4.

Synthesis of Ethyl (*S*)-2-((2-(*tert*-butoxy)-2-oxoethyl)amino)-4-phenylbutanoate (7): A mixture of ethyl (*S*)-2-amino-4-phenylbutanoate (2 g, 8.2 mmol), triethylamine (2.48 g, 24.6 mmol) and *tert*-butylchloroacetate (1.6 g, 10.6 mmol) in DMF (20 mL) was stirred at rt for 48 h. The reaction mixture was poured into ice water and extracted with EtOAc. The organic phase was washed with water and brine, dried (Na_2SO_4), and concentrated to give crude product as pale yellowish oil that was purified by column chromatography (25% EtOAc in pet ether) to give the title compound as pale yellowish oil. Yield: 1.1 g; 42%. LCMS: $(M+H)^+$: 322.1; ^{1}H NMR ($CDCl_3$) δ 7.3 (m, 2H), 7.2 (m, 3H), 4.2 (q, *J* = 7 Hz, 2H), 3.4 (m, 1H), 2.75 (t, *J* = 8 Hz, 2H), 1.95-2.15 (m, 2H), 1.55 (m, 1H), 1.5 (s, 1H), 1.3 (t, *J* = 7 Hz, 3H).

Synthesis of Ethyl (*S*)-2-((2-(*tert*-butoxy)-2-oxoethyl)amino)-4-phenylbutanoate: A solution of the preceding compound **7** (0.5 g, 1.55 mmol) and trifluoroacetic acid (1.18 mL, 15.5 mmol) in CH_2Cl_2 (2.5 mL) at 0 °C was allowed to warm to rt over 4 h. The reaction mixture was concentrated, to give the title compound as a brownish gum. The resulting residue was taken to the next step as such without any further purification. Yield: 0.58 g, 98%. LCMS: $(M+H)^+$: 266.2. ^{1}H NMR (d^{6}-DMSO) δ 7.35 (t, *J* = 7 Hz, 2H), 7.2 (d, *J* = 7 Hz, 3H), 4.2-4.3 (m, 2H), 4.1 (m, 1H), 4.0 (d, *J* = 17 Hz, 1H), 3.95 (d, *J* = 17 Hz, 1H), 2.7-2.8 (m, 1H), 2.55 (m, 1H), 2.05-2.3 (m, 2H), 1.25 (t, *J* = 7 Hz, 3H).

Synthesis of (*S*)-N-(*tert*-butoxycarbonyl)-*N*-(1-ethoxy-1-oxo-4-phenylbutan-2-yl) glycine (8): Boc anhydride (0.69 g; 3.16 mol) was added to a stirred solution of the preceding compound (0.8 g, 2.11 mmol) and triethylamine (0.85 g, 8.44 mmol) in dry THF (10 ml) at 0 °C. The mixture was heated at 70°C for 2 h. After cooling to rt, the reaction mixture was poured

ice water and extracted twice with EtOAc (2 x 50 mL). The combined organic layers were washed with water and brine, dried (Na_2SO_4) and concentrated the title compound as a pale yellowish gum. Yield: 1.0 g; 91 %. LCMS: $(M\text{-}CO_2\text{-isobutylene})^+$: 266.2.

Synthesis of Methyl (2*S*,5*R*)-1-(((*S*)-1-ethoxy-1-oxo-4-phenylbutan-2-yl)glycyl)-5-(p-tolyl)pyrrolidine-2-carboxylate: A solution of propanephosphonic acid anhydride (50% in EtOAc) (2.6 ml, 4.1 mmol) was added to a solution of the preceding compound **8** (0.99 g, 2.73 mmol), methyl (2*S*,5*R*)-5-(p-tolyl)pyrrolidine-2-carboxylate **9** (synthesis of **9** provided in Supporting Information) (0.5 g, 2.28 mmol) and triethylamine (0.0.64 ml, 4.56 mmol) in THF (20 ml) at 0°C. The mixture was warmed to rt over 10 min at 0°C, before being poured into ice water and extracted twice with EtOAc. The combined organic layers were dried over Na_2SO_4 and concentrated to afford the title compound as a brown gummy solid that was purified by flash chromatography (1:1 EtOAc, pet. Ether) to afford the title compound as a pale-yellow oil. Yield: 0.38 g; 30%. LCMS: $(M+H)^+$: 567.2. ^{1}H NMR (d^6-DMSO) δ 7.5-7.6 (m, 2H), 7.25-7.35 (m, 2H), 7.05-7.25 (m, 4H), 5.1 (m, 1H), 4.4 (m, 2H), 3.9 (m, 3H), 3.7 (s, 3H), 3.1 (m, 1H), 2.7 (m, 2H), 2.25 (s, 3H), 1.85 (m, 3H), 1.65 (m, 1H), 1.4 and 1.45 (2s, 9H), 1.2 (m, 1H), 1.05 (m, 3H).

Synthesis of (2*S*,5*R*)-1-(((*S*)-1-carboxy-3-phenylpropyl)glycyl)-5-(*p*-tolyl)pyrrolidine-2-carboxylic acid (10, AD013): Concentrated HCl (1.52 mL) was added to a stirred solution of preceding compound (0.38 g; 0.67 mmol) in 1.5 N HCl (1.9 mL), and the mixture was heated at 60°C for 2 h. After cooling to room temperature and removal of solvent, the residue was purified by reverse phase HPLC (water/acetonitrile gradient with 0.1% TFA method) to afford the title compound as a white solid. Yield: 0.09 g, 32 %. LCMS: $(M+H)^+$: 425.3. ^{1}H NMR (d^4-MeOH) δ 7.5 (d, *J* = 8 Hz, 2H), 7.1-7.35 (m, 7H), 5.0 (t, *J* = 7 Hz, 1H), 4.65 (t, *J* = 9.5 Hz, 1H), 3.7 (d, *J* = 16 Hz, 1H), 3.5 (t, *J* = 6 Hz, 1H), 3.2 (d, *J* = 16 Hz, 1H), 2.6-2.7 (m, 2H), 2.5 (m, 1H), 2.35 (m, 1H), 2.3 (s, 3H), 2.1-2.2 (m, 1H), 1.95-2.1 (m, 1H). ^{13}C NMR (d^4-MeOH) δ 174.0, 173.7, 172.1, 169.4, 142.0, 140.3, 136.7, 135.7, 129.6, 129.2, 128.9, 128.85, 128.8, 128.7, 128.65, 126.6, 126.5, 126.2, 125.6, 61.5, 60.9, 60.1, 59.2, 48.6, 36.2, 33.8, 31.8, 31.6, 29.8, 27.5, 21.1.

Compound dissolution

Compounds were synthesised by CRO, Syngene. Compound stock solutions were prepared at a concentration of 10 mM in DMSO for all compounds except LisW, which was dissolved in distilled H_2O.

ACE Inhibition Assays

Fully glycosylated (D629 and Δ36NJ) human cACE and nACE proteins were expressed in mammalian Chinese hamster ovary (CHO) cells and purified as described previously.[36, 53] In vitro ACE inhibition was assessed using a fluorogenic endpoint assay. A two-fold serial dilution of inhibitors was carried out in ACE assay buffer (100 mM potassium phosphate buffer, pH 8.3, 300 mM NaCl, 10 μM ZnCl2). Enzymes were pre-incubated with inhibitors for 15 min at 22 °C, and reactions were initiated by the addition of Cbz-Phe-His-Leu (Z-FHL, Bachem Ltd., nACE K_m = 600 μM; cACE K_m = 60 μM). Final reactions contained ~1 nM nACE/cACE and 0.5 mM Z-FHL. Each reaction was carried out in triplicate. After incubation at 37 °C for 10 min, the reactions were stopped by the addition of 165 μL of 0.34 M NaOH containing 2 mg/mL of the derivatizing agent o-phthalaldyde. Derivatization was carried out for 10 min at 22 °C and stopped by the addition of 25 μL of 3 M HCl. A fluorescence spectrophotometer (Varian Inc.) was used to measure fluorescent intensities at λex = 360 nm and λem = 485 nm. To determine IC_{50} values, log(inhibitor) vs response (V_i/V_o) (variable slope) curves were fitted to the data using GraphPad Prism where V_i is initial velocity in the presence of inhibitor and V_o is the initial velocity in the absence of inhibitor. IC_{50} values were calculated from n ≥ 2 independent experiments.

NEP Inhibition Assays

The DNA sequence for the ectodomain of human NEP fused to an octahistidine tag and a human growth hormone domain (hGH-8His-NEP)[54] was sub-cloned into pcDNA3.1 and expressed in mammalian CHO cells using the same protocol as for ACE proteins. The secreted glycosylated NEP protein was purified from the harvested OptiMEM expression medium using cobalt-based Talon metal affinity chromatography. The purified protein was concentrated and stored in 20 mM Tris, 150 mM NaCl, pH 7.5 at -20 °C. NEP activity was measured using the MCA-RPPGFSAFK(Dnp)-OH peptide substrate (R&D Systems; NEP K_m = 7 μM) in a

continuous assay format. A two-fold serial dilution of inhibitors was carried out in NEP assay buffer (50 mM Tris pH 8.3, 0.05% Brij-35, 300 mM NaCl, 10 µM $ZnCl_2$). Enzyme and inhibitor were pre-incubated for 15 min at 22°C, and the reaction was initiated by the addition of substrate. Each reaction was carried out in triplicate. Final reactions contained 5 µM of substrate and 0.4 nM of NEP. The increase in fluorescence with time was monitored at λex= 320 nm and λem= 405 nm using a fluorescence spectrophotometer (Varian Inc.) and IC_{50} values were determined as described above for the ACE inhibition assays. IC_{50} values were calculated from n ≥ 2 independent experiments.

X-ray crystallographic studies

Minimally glycosylated nACE and cACE proteins (N389 and G13, respectively) were generated by expression in cultured mammalian CHO cells, and purified to homogeneity as described previously.[53, 55] Purity was assessed using SDS-PAGE and proteins were shown to be >95% pure. ACE was pre-incubated with the ligands for 1 hour (at room temperature for nACE and on ice for cACE) using a 4:1 v/v ratio of protein (5 and 8 mg ml^{-1} nACE and cACE, respectively, in 50 mM HEPES, pH 7.5, 0.1 mM PMSF) and 1 mM inhibitor (10 mM stocks in DMSO of AD011, AD012 and AD013, diluted to 1 mM with water). Hanging drops of 1 µl of the protein-inhibitor complex mixed with 1 µl of reservoir solution were set up. The standard Molecular Dimensions Morpheus A9 condition was used for nACE (30% PEG 550 MME/PEG 20000, 0.1 M Tris/Bicine pH 8.5 and 60 mM divalent cations). The cACE complexes crystallised in 0.1 M MIB buffer pH 4.0 and 5% v/v glycerol, with varying amounts of PEG 3350 (16 % v/v for AD011, and 15 % v/v for both AD012 and AD013).

X-ray diffraction data were collected on stations i04-1 (nACE in complex with AD011, AD012 and AD013, and cACE-AD013), i24 (cACE-AD011) and i03 (cACE-AD012) at the Diamond Light Source (Didcot, UK), with the crystals kept at a constant temperature (100 K) using a nitrogen stream. Images were collected using detectors PILATUS-6M-F (i04-1) and PILATUS3 6M (i24 and i03) (Dectris, Switzerland). Raw data images were indexed and integrated with DIALS,[56] and then scaled using AIMLESS[57] from the CCP4 suite.[58] Initial phases were obtained by molecular replacement with PHASER[59] using N389-nACE PDB code 6F9V[49] and G13-cACE PDB code 6F9T[49] as search models for nACE and cACE, respectively. Further refinement was initially carried out using REFMAC5[60] and then Phenix,[61] with

COOT[62] used for rounds of manual model building. Ligand and water molecules were added based on electron density in the mFo – DFc Fourier difference map. MolProbity[63] was used to help validate the structures. Crystallographic data statistics are summarized in **Table 2**. All figures showing the crystal structures were generated using CCP4mg,[64] and schematic binding interactions are displayed using Ligplot+.[65]

In silico docking

The crystal structure of human NEP in complex with sampatrilat (PDBID: 6XVP) was prepared for modeling calculations using the Protein Preparation Wizard tool in Maestro (Schrodinger, LLC, New York, NY). 3D models of inhibitors were constructed using sampatrilat as a template and prepared for modeling using Maestro's LigPrep module. Initial binding models of AD011, AD012, and AD013 in NEP was generated by Prime minimization of the ligand and the protein within 6 Å of the ligand, using the OPLS3e force field, the variable-dielectric generalized Born (VSGB) solvation model for water, and a dielectric constant of 80. Final binding models were generated using the MM-GBSA minimization of the ligand and NEP binding site within 6Å of the ligand. Modeling figures were produced using PyMOL version 1.8.6.2, Schrodinger, LLC.

ASSOCIATED CONTENT

Supporting information

Supporting information includes additional chemistry experimental details, a table showing RMSD values for overall structures of nACE and cACE in complex with inhibitors, and supporting figures including an overlay of NEP structures illustrating two different inhibitor binding orientations, schematic representation of the overall structures of nACE and cACE in complex with inhibitors, Ligplot representations of lisinopril and LisW binding interactions, and chemical structures of previously reported keto-ACE inhibitors.

Molecular formula strings (CSV)

In silico docking files. NEP-AD011, NEP-AD012 and NEP-AD013 (PDB).

Accession codes

The atomic co-ordinates and structure factors have been deposited in the RCSB Protein Data Bank (www.rcsb.org/pdb) with accession numbers 7Q24 (nACE-AD011), 7Q25 (nACE-AD012), 7Q26 (nACE-AD013), 7Q27 (cACE-AD011), 7Q28 (cACE-AD012) and 7Q29 (cACE-AD013). The atomic co-ordinates and experimental data will be released upon article publication.

AUTHOR INFORMATION

Corresponding Authors

*E-mail: Edward D. Sturrock edward.sturrock@uct.ac.za; Ravi Acharya bsskra@bath.ac.uk

Author Contributions

L.B.A. and G.E.C. contributed equally. L.B.A., G.E.C. and G.S.B. wrote the manuscript. L.B.A., C.J.E. and G.S.B. designed the compounds. L.B.A, G.E.C, C.J.E. and S.L.S. carried out the experimental work. K.C., K.R.A. and E.D.S. supervised the project and edited the manuscript. All authors read and approved the manuscript for publication.

ACKNOWLEDGEMENTS

We thank the scientists at stations i04-1, i24 and i03 (Proposal Number mx17212) of Diamond Light Source, Didcot, Oxfordshire (UK), for their support during X-ray diffraction data collection.

ABBREVIATIONS USED

ACE, Angiotensin-1 converting enzyme; ARBs, angiotensin receptor blockers; Ac-SDKP, N-acetyl-Ser–Asp–Lys–Pro; CHO, Chinese hamster ovary cells; DMSO, dimethyl sulfoxide; Dnp, dinitrophenyl; NEP, Neprilysin; PDB, Protein Data Bank; RAS, renin-angiotensin system.

Competing interests

We declare that there are no conflicts of interest

Funding information

This work was supported by the Medical Research Council (U.K.) Project Grant MR/M026647/1 (to K.R.A.) and by a UK Global Challenge Research Fund grant: START-Synchrotron Techniques for African Research and Technology (Science and Technology Facilities Council grant ST/R002754/1) (to E.D.S.). K.C. gratefully acknowledges the support of the University of Cape Town, South African Medical Research Council, and the South African Research Chairs Initiative of the Department Science and Innovation administered through the South African National Research Foundation.

References

1. Oparil, S.; Schmieder, R. E. New approaches in the treatment of hypertension. *Circ Res* **2015,** 116, 1074-1095.
2. Arendse, L. B.; Danser, A. H. J.; Poglitsch, M.; Touyz, R. M.; Burnett, J. C., Jr.; Llorens-Cortes, C.; Ehlers, M. R.; Sturrock, E. D. Novel therapeutic approaches targeting the renin-angiotensin system and associated peptides in hypertension and heart failure. *Pharmacol Rev* **2019,** 71, 539-570.
3. Coric, P.; Turcaud, S.; Meudal, H.; Roques, B. P.; FournieZaluski, M. C. Optimal recognition of neutral endopeptidase and angiotensin-converting enzyme active sites by mercaptoacyldipeptides as a means to design potent dual inhibitors. *J Med Chem* **1996,** 39, 1210-1219.
4. Delaney, N. G.; Barrish, J. C.; Neubeck, R.; Natarajan, S.; Cohen, M.; Rovnyak, G. C.; Huber, G.; Murugesan, N.; Girotra, R.; Siebermcmaster, E.; Robl, J. A.; Asaad, M. M.; Cheung, H. S.; Bird, J. E.; Waldron, T.; Petrillo, E. W. Mercaptoacyl dipeptides as dual inhibitors of angiotensin-converting enzyme and neutral endopeptidase. Preliminary structure-activity studies. *Bioorg Med Chem Lett* **1994,** 4, 1783-1788.
5. Fournie-Zaluski, M. C.; Coric, P.; Thery, V.; Gonzalez, W.; Meudal, H.; Turcaud, S.; Michel, J. B.; Roques, B. P. Design of orally active dual inhibitors of neutral endopeptidase and angiotensin-converting enzyme with long duration of action. *J Med Chem* **1996,** 39, 2594-2608.
6. Robl, J. A.; Sun, C. Q.; Stevenson, J.; Ryono, D. E.; Simpkins, L. M.; Cimarusti, M. P.; Dejneka, T.; Slusarchyk, W. A.; Chao, S.; Stratton, L.; Misra, R. N.; Bednarz, M. S.; Asaad, M. M.; Cheung, H. S.; Abboa-Offei, B. E.; Smith, P. L.; Mathers, P. D.; Fox, M.; Schaeffer, T. R.; Seymour, A. A.; Trippodo, N. C. Dual metalloprotease inhibitors: mercaptoacetyl-based fused heterocyclic dipeptide mimetics as inhibitors of angiotensin-converting enzyme and neutral endopeptidase. *J Med Chem* **1997,** 40, 1570-1577.
7. Campese, V. M.; Lasseter, K. C.; Ferrario, C. M.; Smith, W. B.; Ruddy, M. C.; Grim, C. E.; Smith, R. D.; Vargas, R.; Habashy, M. F.; Vesterqvist, O.; Delaney, C. L.; Liao, W. C. Omapatrilat versus lisinopril - Efficacy and neurohormonal profile in salt-sensitive hypertensive patients. *Hypertension* **2001,** 38, 1342-1348.
8. Intengan, H. D.; Schiffrin, E. L. Vasopeptidase inhibition has potent effects on blood pressure and resistance arteries in stroke-prone spontaneously hypertensive rats. *Hypertension* **2000,** 35, 1221-1225.

9. McClean, D. R.; Ikram, H.; Garlick, A. H.; Richards, A. M.; Nicholls, M. G.; Crozier, I. G. The clinical, cardiac, renal, arterial and neurohormonal effects of omapatrilat, a vasopeptidase inhibitor, in patients with chronic heart failure. *J Am Coll Cardiol* **2000,** 36, 479-486.
10. Mitchell, G. F.; Izzo, J. L.; Lacourciere, Y.; Ouellet, J. P.; Neutel, J.; Qian, C. L.; Kerwin, L. J.; Block, A. J.; Pfeffer, M. A. Omapatrilat reduces pulse pressure and proximal aortic stiffness in patients with systolic hypertension - Results of the conduit hemodynamics of Omapatrilat International Research Study. *Circulation* **2002,** 105, 2955-2961.
11. Pu, Q.; Touyz, R. M.; Schiffrin, E. L. Comparison of angiotensin-converting enzyme (ACE), neutral endopeptidase (NEP) and dual ACE/NEP inhibition on blood pressure and resistance arteries of deoxycorticosterone acetate-salt hypertensive rats. *J Hypertens* **2002,** 20, 899-907.
12. Rouleau, J. L.; Pfeffer, M. A.; Stewart, D. J.; Isaac, D.; Sestier, F.; Kerut, E. K.; Porter, C. B.; Proulx, G.; Qian, C. L.; Block, A. J.; Investigators, I. Comparison of vasopeptidase inhibitor, omapatrilat, and lisinopril on exercise tolerance and morbidity in patients with heart failure: IMPRESS randomised trial. *Lancet* **2000,** 356, 615-620.
13. Trippodo, N. C.; Fox, M.; Monticello, T. M.; Panchal, B. C.; Asaad, M. M. Vasopeptidase inhibition with omapatrilat improves cardiac geometry and survival in cardiomyopathic hamsters more than does ACE inhibition with captopril. *J Cardiovasc Pharmacol* **1999,** 34, 782-790.
14. Trippodo, N. C.; Robl, J. A.; Asaad, M. M.; Fox, M.; Panchal, B. C.; Schaeffer, T. R. Effects of omapatrilat in low, normal, and high renin experimental hypertension. *Am J Hypertens* **1998,** 11, 363-372.
15. Coats, A. J. S. Omapatrilat - the story of Overture and Octave. *Int J Cardiol* **2002,** 86, 1-4.
16. Kostis, J. B.; Packer, M.; Black, H. R.; Schmieder, R.; Henry, D.; Levy, E. Omapatrilat and enalapril in patients with hypertension: the Omapatrilat Cardiovascular Treatment vs. Enalapril (OCTAVE) trial. *Am J Hypertens* **2004,** 17, 103-111.
17. Packer, M.; Califf, R. M.; Konstam, M. A.; Krum, H.; McMurray, J. J.; Rouleau, J. L.; Swedberg, K.; Grp, O. S. Comparison of omapatrilat chronic and enalapril in patients with heart failure - The omapatrilat versus enalapril randomized trial of utility in reducing events (OVERTURE). *Circulation* **2002,** 106, 920-926.
18. Zanchi, A.; Maillard, M.; Burnier, M. Recent clinical trials with omapatrilat: New developments. *Curr Hypertens Rep* **2003,** 5, 346-352.
19. Byrd, J. B.; Adam, A.; Brown, N. J. Angiotensin-converting enzyme inhibitor-associated angioedema. *Immunol Allergy Clin North Am* **2006,** 26, 725-737.
20. Molinaro, G.; Cugno, M.; Perez, E.; Lepage, Y.; Gervais, N.; Agostoni, A.; Adam, A. Angiotensin-converting enzyme inhibitor-associated angioedema is characterized by a slower degradation of des-Arginine(9)-bradykinin. *J Pharmacol Exp Ther* **2002,** 303, 232-237.
21. Fox, A. J.; Lalloo, U. G.; Belvisi, M. G.; Bernareggi, M.; Chung, K. F.; Barnes, P. J. Bradykinin-evoked sensitization of airway sensory nerves: A mechanism for ACE-inhibitor cough. *Nat Med* **1996,** 2, 814-817.
22. Bernstein, K. E.; Shen, X. Z.; Gonzalez-Villalobos, R. A.; Billet, S.; Okwan-Duodu, D.; Ong, F. S.; Fuchs, S. Different in vivo functions of the two catalytic domains of angiotensin-converting enzyme (ACE). *Curr Opin Pharmacol* **2011,** 11, 105-111.
23. Fuchs, S.; Xiao, H. D.; Hubert, C.; Michaud, A.; Campbell, D. J.; Adams, J. W.; Capecchi, M. R.; Corvol, P.; Bernstein, K. E. Angiotensin-converting enzyme C-terminal

catalytic domain is the main site of angiotensin I cleavage in vivo. *Hypertension* **2008,** 51, 267-274.
24. Junot, C.; Gonzales, M. F.; Ezan, E.; Cotton, J.; Vazeux, G.; Michaud, A.; Azizi, M.; Vassiliou, S.; Yiotakis, A.; Corvol, P.; Dive, V. RXP 407, a selective inhibitor of the N-domain of angiotensin I-converting enzyme, blocks in vivo the degradation of hemoregulatory peptide acetyl-Ser-Asp-Lys-Pro with no effect on angiotensin I hydrolysis. *J Pharmacol Exp Ther* **2001,** 297, 606-611.
25. van Esch, J. H. M.; Tom, B.; Dive, V.; Batenburg, W. W.; Georgiadis, D.; Yiotakis, A.; van Gool, J. M. G.; de Bruijn, R. J. A.; de Vries, R.; Danser, A. H. J. Selective angiotensin-converting enzyme c-domain inhibition is sufficient to prevent angiotensin I-induced vasoconstriction. *Hypertension* **2005,** 45, 120-125.
26. Fuchs, S.; Xiao, H. D.; Cole, J. M.; Adams, J. W.; Frenzel, K.; Michaud, A.; Zhao, H.; Keshelava, G.; Capecchi, M. R.; Corvol, P.; Bernstein, K. E. Role of the N-terminal catalytic domain of angiotensin-converting enzyme investigated by targeted inactivation in mice. *J Biol Chem* **2004,** 279, 15946-15953.
27. Dive, V.; Cotton, J.; Yiotakis, A.; Michaud, A.; Vassiliou, S.; Jiracek, J.; Vazeux, G.; Chauvet, M. T.; Cuniasse, P.; Corvol, P. RXP 407, a phosphinic peptide, is a potent inhibitor of angiotensin I converting enzyme able to differentiate between its two active sites. *Proc Natl Acad Sci U S A* **1999,** 96, 4330-4335.
28. Douglas, R. G.; Sharma, R. K.; Masuyer, G.; Lubbe, L.; Zamora, I.; Acharya, K. R.; Chibale, K.; Sturrock, E. D. Fragment-based design for the development of N-domain-selective angiotensin-1-converting enzyme inhibitors. *Clin Sci (Lond)* **2014,** 126, 305-313.
29. Fienberg, S.; Cozier, G. E.; Acharya, K. R.; Chibale, K.; Sturrock, E. D. The design and development of a potent and selective novel diprolyl derivative that binds to the N-domain of angiotensin-I converting enzyme. *J Med Chem* **2018,** 61, 344-359.
30. Georgiadis, D.; Beau, F.; Czarny, B.; Cotton, J.; Yiotakis, A.; Dive, V. Roles of the two active sites of somatic angiotensin-converting enzyme in the cleavage of angiotensin I and bradykinin - Insights from selective inhibitors. *Circul Res* **2003,** 93, 148-154.
31. Georgiadis, D.; Cuniasse, P.; Cotton, J.; Yiotakis, A.; Dive, V. Structural determinants of RXPA380, a potent and highly selective inhibitor of the angiotensin-converting enzyme C-domain. *Biochemistry* **2004,** 43, 8048-8054.
32. Nchinda, A. T.; Chibale, K.; Redelinghuys, P.; Sturrock, E. D. Synthesis and molecular modeling of a lisinopril-tryptophan analogue inhibitor of angiotensin I-converting enzyme. *Bioorg Med Chem Lett* **2006,** 16, 4616-4619.
33. Watermeyer, J. M.; Kroger, W. L.; O'Neill, H. G.; Sewell, B. T.; Sturrock, E. D. Probing the basis of domain-dependent inhibition using novel ketone inhibitors of Angiotensin-converting enzyme. *Biochemistry* **2008,** 47, 5942-5950.
34. Corradi, H. R.; Chitapi, I.; Sewell, B. T.; Georgiadis, D.; Dive, V.; Sturrock, E. D.; Acharya, K. R. The structure of testis angiotensin-converting enzyme in complex with the C-domain specific inhibitor RXPA380. *Biochemistry* **2007,** 46, 5473-5478.
35. Cozier, G. E.; Lubbe, L.; Sturrock, E. D.; Acharya, K. R. ACE-domain selectivity extends beyond direct interacting residues at the active site. *Biochem J* **2020,** 477, 1241-1259.
36. Kroger, W. L.; Douglas, R. G.; O'Neill, H. G.; Dive, V.; Sturrock, E. D. Investigating the domain specificity of phosphinic inhibitors RXPA380 and RXP407 in angiotensin-converting enzyme. *Biochemistry* **2009,** 48, 8405-8412.

37. Lubbe, L.; Sewell, B. T.; Sturrock, E. D. The influence of angiotensin converting enzyme mutations on the kinetics and dynamics of N-domain selective inhibition. *FEBS J* **2016,** 283, 3941-3961.
38. Sturrock, E. D.; Lubbe, L.; Cozier, G. E.; Schwager, S. L. U.; Arowolo, A. T.; Arendse, L. B.; Belcher, E.; Acharya, K. R. Structural basis for the C-domain-selective angiotensin-converting enzyme inhibition by bradykinin-potentiating peptide b (BPPb). *Biochem J* **2019,** 476, 1553-1570.
39. Watermeyer, J. M.; Kroger, W. L.; O'Neill, H. G.; Sewell, B. T.; Sturrock, E. D. Characterization of domain-selective inhibitor binding in angiotensin-converting enzyme using a novel derivative of lisinopril. *Biochem J* **2010,** 428, 67-74.
40. Sharp, S.; Poglitsch, M.; Zilla, P.; Davies, N. H.; Sturrock, E. D. Pharmacodynamic effects of C-domain-specific ACE inhibitors on the renin-angiotensin system in myocardial infarcted rats. *J Renin Angiotensin Aldosterone Syst* **2015,** 16, 1149-1158.
41. Burger, D.; Reudelhuber, T. L.; Mahajan, A.; Chibale, K.; Sturrock, E. D.; Touyz, R. M. Effects of a domain-selective ACE inhibitor in a mouse model of chronic angiotensin II-dependent hypertension. *Clin Sci (Lond)* **2014,** 127, 57-63.
42. Azizi, M.; Massien, C.; Michaud, A.; Corvol, P. In vitro and in vivo inhibition of the 2 active sites of ACE by omapatrilat, a vasopeptidase inhibitor. *Hypertension* **2000,** 35, 1226-1231.
43. Cozier, G. E.; Arendse, L. B.; Schwager, S. L.; Sturrock, E. D.; Acharya, K. R. Molecular basis for multiple omapatrilat binding sites within the ACE C-domain: implications for drug design. *J Med Chem* **2018,** 61, 10141-10154.
44. Alves-Lopes, R.; Montezano, A. C.; Neves, K. B.; Harvey, A.; Rios, F. J.; Skiba, D. S.; Arendse, L. B.; Guzik, T. J.; Graham, D.; Poglitsch, M.; Sturrock, E.; Touyz, R. M. Selective Inhibition of the C-Domain of ACE (Angiotensin-Converting Enzyme) Combined With Inhibition of NEP (Neprilysin): A Potential New Therapy for Hypertension. *Hypertension* **2021,** 78, 604-616.
45. Oefner, C.; D'Arcy, A.; Hennig, M.; Winkler, F. K.; Dale, G. E. Structure of human neutral endopeptidase (Neprilysin) complexed with phosphoramidon. *J Mol Biol* **2000,** 296, 341-9.
46. Sharma, U.; Cozier, G. E.; Sturrock, E. D.; Acharya, K. R. Molecular basis for omapatrilat and sampatrilat binding to neprilysin—implications for dual inhibitor design with angiotensin-converting enzyme. *J Med Chem* **2020,** 63, 5488-5500.
47. Oefner, C.; Roques, B. P.; Fournie-Zaluski, M. C.; Dale, G. E. Structural analysis of neprilysin with various specific and potent inhibitors. *Acta Crystallogr D Struct Biol* **2004,** 60, 392-6.
48. Iwasaki, G.; Kimura, R.; Numao, N.; Kondo, K. A practical and diastereoselective synthesis of angiotensin converting enzyme inhibitors. *Chem Pharm Bull* **1989,** 37, 280-283.
49. Cozier, G. E.; Schwager, S. L.; Sharma, R. K.; Chibale, K.; Sturrock, E. D.; Acharya, K. R. Crystal structures of sampatrilat and sampatrilat-Asp in complex with human ACE - a molecular basis for domain selectivity. *FEBS J* **2018,** 285, 1477-1490.
50. Corradi, H. R.; Schwager, S. L. U.; Nchinda, A. T.; Sturrock, E. D.; Acharya, K. R. Crystal structure of the N domain of human somatic angiotensin I-converting enzyme provides a structural basis for domain-specific inhibitor design. *J Mol Biol* **2006,** 357, 964-974.
51. Natesh, R.; Schwager, S. L. U.; Sturrock, E. D.; Acharya, K. R. Crystal structure of the human angiotensin-converting enzyme–lisinopril complex. *Nature* **2003,** 421, 551-554.

52. Shindo, M.; Sato, Y.; Koretsune, R.; Yoshikawa, T.; Matsumoto, K.; Itoh, K.; Shishido, K. Synthesis of alpha,alpha-dibromo esters as precursors of ynolates. *Chem Pharm Bull (Tokyo)* **2003,** 51, 477-8.
53. Gordon, K.; Redelinghuys, P.; Schwager, S. L.; Ehlers, M. R.; Papageorgiou, A. C.; Natesh, R.; Acharya, K. R.; Sturrock, E. D. Deglycosylation, processing and crystallization of human testis angiotensin-converting enzyme. *Biochem J* **2003,** 371, 437-442.
54. Guan, H.; Chow, K. M.; Shah, R.; Rhodes, C. J.; Hersh, L. B. Degradation of islet amyloid polypeptide by neprilysin. *Diabetologia* **2012,** 55, 2989-2998.
55. Anthony, C. S.; Corradi, H. R.; Schwager, S. L.; Redelinghuys, P.; Georgiadis, D.; Dive, V.; Acharya, K. R.; Sturrock, E. D. The N domain of human angiotensin-I-converting enzyme: the role of N-glycosylation and the crystal structure in complex with an N domain-specific phosphinic inhibitor, RXP407. *J Biol Chem* **2010,** 285, 35685-35693.
56. Waterman, D. G.; Winter, G.; Gildea, R. J.; Parkhurst, J. M.; Brewster, A. S.; Sauter, N. K.; Evans, G. Diffraction-geometry refinement in the DIALS framework. *Acta Crystallogr D Biol Crystallogr* **2016,** 72, 558-575.
57. Evans, P. R.; Murshudov, G. N. How good are my data and what is the resolution? *Acta Crystallogr D Biol Crystallogr* **2013,** 69, 1204-1214.
58. Collaborative Computational Project Number 4. The CCP4 suite: programs for protein crystallography. *Acta Crystallogr D Biol Crystallogr* **1994,** 50, 760-763.
59. McCoy, A. J.; Grosse-Kunstleve, R. W.; Adams, P. D.; Winn, M. D.; Storoni, L. C.; Read, R. J. Phaser crystallographic software. *J Appl Crystallogr* **2007,** 40, 658-674.
60. Murshudov, G. N.; Vagin, A. A.; Dodson, E. J. Refinement of macromolecular structures by the maximum-likelihood method. *Acta Crystallogr D Biol Crystallogr* **1997,** 53, 240-255.
61. Adams, P. D.; Afonine, P. V.; Bunkoczi, G.; Chen, V. B.; Davis, I. W.; Echols, N.; Headd, J. J.; Hung, L. W.; Kapral, G. J.; Grosse-Kunstleve, R. W.; McCoy, A. J.; Moriarty, N. W.; Oeffner, R.; Read, R. J.; Richardson, D. C.; Richardson, J. S.; Terwilliger, T. C.; Zwart, P. H. PHENIX: a comprehensive Python-based system for macromolecular structure solution. *Acta Crystallogr D Biol Crystallogr* **2010,** 66, 213-221.
62. Emsley, P.; Cowtan, K. Coot: model-building tools for molecular graphics. *Acta Crystallogr D Biol Crystallogr* **2004,** 60, 2126-2132.
63. Chen, V. B.; Arendall, W. B., 3rd; Headd, J. J.; Keedy, D. A.; Immormino, R. M.; Kapral, G. J.; Murray, L. W.; Richardson, J. S.; Richardson, D. C. MolProbity: all-atom structure validation for macromolecular crystallography. *Acta Crystallogr D Biol Crystallogr* **2010,** 66, 12-21.
64. McNicholas, S.; Potterton, E.; Wilson, K. S.; Noble, M. E. Presenting your structures: the CCP4mg molecular-graphics software. *Acta Crystallogr D Biol Crystallogr* **2011,** 67, 386-394.
65. Laskowski, R. A.; Swindells, M. B. LigPlot+: multiple ligand-protein interaction diagrams for drug discovery. *J Chem Inf Model* **2011,** 51, 2778-2786.

Table of Contents graphic